Differential Affinity and Catalytic Activity of CheZ in *E. coli* Chemotaxis

Siebe B. van Albada*, Pieter Rein ten Wolde

FOM Institute for Atomic and Molecular Physics, Amsterdam, The Netherlands

Abstract

Push–pull networks, in which two antagonistic enzymes control the activity of a messenger protein, are ubiquitous in signal transduction pathways. A classical example is the chemotaxis system of the bacterium *Escherichia coli*, in which the kinase CheA and the phosphatase CheZ regulate the phosphorylation level of the messenger protein CheY. Recent experiments suggest that both the kinase and the phosphatase are localized at the receptor cluster, and Vaknin and Berg recently demonstrated that the spatial distribution of the phosphatase can markedly affect the dose–response curves. We argue, using mathematical modeling, that the canonical model of the chemotaxis network cannot explain the experimental observations of Vaknin and Berg. We present a new model, in which a small fraction of the phosphatase is localized at the receptor cluster, while the remainder freely diffuses in the cytoplasm; moreover, the phosphatase at the cluster has a higher binding affinity for the messenger protein and a higher catalytic activity than the phosphatase in the cytoplasm. This model is consistent with a large body of experimental data and can explain many of the experimental observations of Vaknin and Berg. More generally, the combination of differential affinity and catalytic activity provides a generic mechanism for amplifying signals that could be exploited in other two-component signaling systems. If this model is correct, then a number of recent modeling studies, which aim to explain the chemotactic gain in terms of the activity of the receptor cluster, should be reconsidered.

Citation: van Albada SB, ten Wolde PR (2009) Differential Affinity and Catalytic Activity of CheZ in *E. coli* Chemotaxis. PLoS Comput Biol 5(5): e1000378. doi:10.1371/journal.pcbi.1000378

Editor: Christopher Rao, University of Illinois at Urbana-Champaign, United States of America

Received April 28, 2008; **Accepted** April 1, 2009; **Published** May 8, 2009

Copyright: © 2009 van Albada, ten Wolde. This is an open-access article distributed under the terms of the Creative Commons Attribution License, which permits unrestricted use, distribution, and reproduction in any medium, provided the original author and source are credited.

Funding: This work is part of the research program of the Stichting voor Fundamenteel Onderzoek der Materie (FOM), which is financially supported by the Nederlandse Organisatie voor Wetenschappelijk Onderzoek (NWO). The funders had no role in study design, data collection and analysis, decision to publish, or preparation of the manuscript.

Competing Interests: The authors have declared that no competing interests exist.

* E-mail: siebevanalbada@gmail.com

Introduction

The protein network that controls chemotaxis of *Escherichia coli* is arguably the most-studied and best-characterized signal transduction pathway. Its relative simplicity makes it an ideal model system for studying signal amplification, integration, transduction, and adaptation. The network consists of three parts: i) a cluster of receptors at the cell membrane, which detects the extracellular ligand; ii) the intracellular signaling pathway, which transmits the signal from the receptor cluster to the flagellar motors; iii) the network that controls the response of the flagellar motors. The intracellular signaling pathway is a push-pull network that consists of a kinase, CheA, that phosphorylates the messenger protein CheY and a phosphatase, CheZ, that dephosphorylates the phosphorylated messenger protein $CheY_p$. In wild-type cells, CheA is localized exclusively at the receptor cluster, and also CheZ is predominantly localized at the receptor cluster [1]. Recently, however, Vaknin and Berg studied mutants in which CheZ can no longer bind the receptor cluster, as a result of which it is uniformly distributed in the cytoplasm [2]. They observed that the response of the intracellular signaling pathway of these mutant cells differs strongly from that of wild-type cells. Inspired by this observation, we recently performed a mathematical modeling study of a canonical push-pull network, which showed that the spatial distribution of the antagonistic enzymes by itself can have a dramatic effect on the response [3]. Our study also showed, however, that the effect depends upon the regime in which the network operates. Here, we first address by detailed mathematical analysis of the canonical model of the *E. coli* chemotaxis network whether the difference in response between wild-type and CheZ mutant cells can be explained by the different spatial distribution of CheZ in these cells. We find that this is not the case; also realistic changes in parameters such as rate constants and protein concentrations do not seem sufficient to explain the difference in response. We then consider two refinements to the canonical model. First, we study the effect of cooperative dephosphorylation of $CheY_p$ by CheZ [4–7]. Next, we consider a refined model of the intracellular chemotaxis network of *E. coli*, in which a small fraction of CheZ is localized at the receptor cluster, while the remainder is distributed in the cytoplasm. This model, which is supported by a wealth of experimental data, can explain many of the experimental observations of Vaknin and Berg [2], and it provides a novel mechanism for signal amplification.

The canonical model of the intracellular chemotaxis network of *E. coli* is described by the following set of chemical reactions:

$$A \xrightarrow{\beta k_0} A_p \tag{1}$$

$$A_p + Y \underset{k_2}{\overset{k_1}{\rightleftharpoons}} A_pY \xrightarrow{k_3} A + Y_p \tag{2}$$

$$Y_p + Z \underset{k_5}{\overset{k_4}{\rightleftharpoons}} Y_pZ \xrightarrow{k_6} Y + Z \tag{3}$$

In this network, the phosphorylated form of the messenger, $CheY_p$ (Y_p), transmits the signal from the receptor cluster to the

Author Summary

In both prokaryotes and eukaryotes, extra- and intracellular signals are often processed by biochemical networks in which two enzymes together control the activity of a messenger protein via opposite modification reactions. A well-known example is the chemotaxis network of *Escherichia coli* that controls the swimming behavior of the bacterium in response to chemical stimuli. Recent experiments suggest that the two counteracting enzymes in this network are colocalized at the receptor cluster, while experiments by Vaknin and Berg indicate that the spatial distribution of the enzymes by itself can markedly affect the response of the network. We argue using mathematical modeling that the most widely used model of the chemotaxis network is inconsistent with these experimental observations. We then present an alternative model in which part of one enzyme is colocalized with the other enzyme at the receptor cluster, while the remainder freely diffuses in the cytoplasm; moreover, the fraction at the cluster both binds more strongly to the messenger protein and modifies it faster. This model is consistent with a large number of experimental observations and provides a generic mechanism for amplifying signals.

flagellar motors. The phosphorylation level of CheY is regulated by a kinase CheA (A) and a phosphatase CheZ (Z). $CheY_p$ also exhibits autophosphorylation and autodephosphorylation, but these reactions are much slower than phosphorylation by CheA and dephosphorylation by CheZ, respectively. The input to the signal transduction pathway is βk_0, where β is a parameter between zero and one that reflects the activity of the receptor cluster and k_0 denotes the maximum rate of autophosphorylation of CheA. The value of β depends on the ligand concentration [L]: $\beta \equiv \beta([L])$; β shifts to lower (higher) values upon the addition of attractant (repellent). In order for *E. coli* to adapt to a changing ligand concentration, the activity of the receptor cluster, β, is also modulated by the methylation and demethylation enzymes CheR and CheB, respectively.

In wild-type *E. coli* cells, not only CheA, but also CheZ is localized at the receptor cluster [1]. In these cells, CheZ is anchored to the receptor cluster by CheA [8,9]. In a recent experiment, Vaknin and Berg compared the response of wild-type cells to that of CheZ mutant cells, in which CheZ does not bind to CheA, but diffuses in the cytoplasm [2]. They studied the response of the chemotaxis network by measuring the interaction between CheZ and $CheY_p$ using FRET imaging. While the input of the network was thus the concentration of ligand, the measured output was proportional to the total, integrated concentration of $CheY_p$ bound to CheZ, $[Y_pZ]$ (see also Eq. 3).

Vaknin and Berg found that the colocalization of the antagonistic enzymes has a marked effect on the dose-response curve [2]. In wild-type cells, in which CheA and CheZ are colocalized at the receptor cluster, the response of $[Y_pZ]$ to changes in the concentration of the attractant serine is more sensitive than in mutant cells, in which CheZ is distributed in the cytoplasm. Moreover, in *cheRcheB* cells, which lack the methylation and demethylation enzymes, the response to the addition of serine is also sharper when CheA and CheZ are colocalized at the receptor cluster [2].

In the next section, we show that the experiments of Vaknin and Berg [2] impose strong constraints on any model that aims to describe the intracellular chemotaxis network. In the subsequent section, we argue that the canonical model does not meet these constraints: neither changes in the spatial distribution of CheZ, nor realistic changes in the rate constants and protein concentrations seem sufficient to explain the differences in the response curves of the mutant and wild-type cells. Indeed, we argue that the experiments of Vaknin and Berg demonstrate that the canonical model needs to be augmented.

In the subsequent sections, we present two refined models of the intracellular chemotaxis network of *E. coli*, which both can explain the difference in response between wild-type cells and CheZ mutant cells, as measured by Vaknin and Berg [2]. The first model assumes that 1) in wild-type cells, CheZ is localized at the cluster, while in the CheZ mutant cells, CheZ freely diffuses in the cytoplasm; 2) CheZ in wild-type cells has a higher phosphatase activity than CheZ in the CheZ mutant cells, as suggested by the observation of Wang and Matsumura that interactions of CheZ with CheA enhance its phosphatase activity [10]; 3) CheZ in wild-type cells acts non-cooperatively, while CheZ in the mutant cells acts cooperatively, as motivated by the experimental observations of [4,6,7]. While this model can describe the FRET response curves as measured by Vaknin and Berg [2], it assumes that in wild-type cells *all CheZ proteins* are bound at the cluster. However, the experiments of Vaknin and Berg show that in wild-type cells, only a small fraction of CheZ is bound at the receptor cluster; the remainder freely diffuses in the cytoplasm [2].

In the next section, we therefore present an alternative model. The key ingredients of this model are: 1) in wild-type cells, a small, yet significant, fraction of CheZ is bound to the receptor cluster, while the remainder freely diffuses in the cytoplasm [2]; 2) the fraction of CheZ at the cluster has a higher binding affinity for the substrate CheY than that of cytosolic CheZ; 3) the catalytic activity of CheZ bound to the cluster is higher than that of CheZ in the cytoplasm. This model bears similarities to that recently proposed by Lipkow [11], although our model neither requires oligomerization of CheZ at the receptor cluster nor shuttling of CheZ between the cytoplasm and the receptor cluster. In the section *Differential affinity and catalytic activity* we show using a simplified model how the combination of differential binding affinity and differential catalytic activity provides a novel mechanism for amplifying signals: As the activity of the receptor cluster and hence that of the kinase CheA is increased from zero and CheY becomes phosphorylated, $CheY_p$ first binds CheZ at the receptor cluster; only when CheZ at the receptor cluster is saturated, does $CheY_p$ bind CheZ in the cytoplasm; since CheZ at the cluster has a higher catalytic activity than CheZ in the cytoplasm, the response of $CheY_p$ is sigmoidal. Finally, we also incorporate cooperative binding of $CheY_p$ to CheZ [5–7] into the model and show that this model can explain the response of *E. coli* to changes in serine concentration, as measured by Vaknin and Berg [2].

Results

Decomposing the response

Vaknin and Berg performed experiments on four bacterial strains: wild-type cells, *cheRcheB* cells lacking the methylation and demethylation enzymes CheR and CheB, CheZ mutant cells, and CheZ mutant cells lacking CheR and CheB [2]. Analysis of their dose-response curves $[Y_pZ]([L])$ (the concentration of $CheY_p$-CheZ—a $CheY_p$ molecule bound to a CheZ dimer—as a function of the ligand concentration L) is complicated by the fact that they are determined by both the response of the receptor cluster, βk_0, to the change in the ligand concentration, [L], and by the response of the intra-cellular signaling pathway, $[Y_pZ]$, to changes in the activity of the receptor cluster, βk_0. However, these two networks

can be viewed as two independent modules connected in series, which can be analyzed separately, as we discuss below. Moreover, this modularity means that the dose-response curves, $[Y_pZ]([L])$, of the four strains can be obtained by multiplying the response curves of the two modules.

The first module is the receptor cluster. Its activity, β, depends upon the concentration of ligand, [L], and upon the methylation states of the receptors, which is controlled by the methylation and demethylation enzymes CheR and CheB, respectively. However, the dynamics of receptor methylation and demethylation by CheR and CheB are much slower than that of receptor-ligand (un)binding and phosphorylation and dephosphorylation of CheY; in fact, this separation of time scales allows *E. coli* to both respond and adapt to a changing ligand concentration. This separation of time scales also makes it possible to model the response to ligand at short time scales without explicitly taking into account the (de)methylation dynamics; the absence of CheR and CheB in *cheRcheB* cells, will lead to different methylation states of the receptors, yet can be modeled implicitly by taking different functional forms for $\beta k_0([L])$. For wild-type cells, the response of the cluster is thus characterized by the response function $\beta k_0^{RB^+}([L])$, while for *cheRcheB* cells, the response is described by $\beta k_0^{RB^-}([L])$.

The second module of the chemotaxis network, the intracellular signal transduction pathway, is described by the set of reactions in Equations 1–3. The input of this network is βk_0, while the output is the concentration of $CheY_p$, $[Y_p]$, or, as in the experiments of Vaknin and Berg, the total concentration of $CheY_p$ bound to CheZ, $[Y_pZ]$ [2]. The response curve of this network, $[Y_pZ](\beta k_0)$, depends upon the nature of CheZ, and will thus be different for wild-type cells and CheZ mutant cells. Importantly, $[Y_pZ](\beta k_0)$ is independent of the methylation states of the receptors. We assume that $[Y_pZ](\beta k_0)$ also does not depend upon the presence of CheB, although phosphorylated CheA can phosphorylate not only CheY but also CheB, leading to another form of adaptation on a time scale longer than that of the response; we will come back to this in the *Discussion* section. Thus, we assume that $[Y_pZ](\beta k_0)$ of *cheRcheB* cells is the same as that of wild-type cells; the absence of CheR and CheB in *cheRcheB* cells only affects $\beta k_0([L])$. Hence, the response of the intra-cellular signaling pathway in wild-type cells is characterized by the response function $[Y_pZ]^{Z^{wt}}(\beta k_0)$, while the response of CheZ mutant cells is characterized by $[Y_pZ]^{Z^*}[\beta k_0]$.

If the receptor cluster and the intracellular chemotaxis pathway indeed behave as two independent modules connected in series, then the response function $(Y_pZ)([L])$ should be given by the composite function $[Y_pZ](\beta k_0([L]))$. Hence, the response function of the four strains in Ref. [2] should be of the form: $[Y_pZ]^{Z^*,Z^{wt}}(\beta k_0^{RB\pm}([L]))$. As we show in Figure 1 of Text S1, the experiments of Vaknin and Berg on the four different strains provide strong evidence for the hypothesis that the receptor cluster and the intracellular network are indeed two independent modules connected in series. Yet, these experiments do not uniquely prescribe how the overall response is decomposed. This is illustrated in Figure 1, which show the response curves of three different models, indicated by different colors, that all can explain the dose-response curves of Figure 1A. Each model consists of the functions $(Y_pZ)^{Z^{wt}}(\beta k_0)$ and $(Y_pZ)^{Z^*}(\beta k_0)$ (Figure 1B), corresponding to wild-type and CheZ mutant cells respectively, and the functions $\beta k_0^{RB^+}([L])$ and $\beta k_0^{RB^-}([L])$ (Figure 1C), corresponding to cells containing CheR and CheB and *cheRcheB* cells lacking CheR and CheB, respectively. For each model, the four composite functions $[Y_pZ]^{\{Z^*,Z^{wt}\}}(\beta k_0^{RB\pm}([L]))$ exactly reproduce the four dose-response curves of Figure 1A. Model I (red lines and points) relies on the assumption that $[Y_pZ]^{Z^*}(\beta k_0)$ is a straight line over the concentration range of interest (see Figure 1B). This means that $\beta k_0^{RB-}([L])$ and $\beta k_0^{RB^+}([L])$ are proportional to $[Y_pZ]([L])$ of CheZ mutant cells lacking CheR and CheB and CheZ mutant cells containing CheR and CheB, respectively; this can be verified by comparing Figure 1A to Figure 1C. The experiments of Vaknin and Berg [2] now fully determine the function $[Y_pZ]^{Z^{wt}}(\beta k_0)$, which can be constructed from $\beta k_0^{RB^+}([L])$ and $[Y_pZ]([L])$ of the wild-type cells, and $\beta k_0^{RB^-}([L])$ and $[Y_pZ]([L])$ of the *cheRcheB* cells (see Figure 1B); this function has a strongly convex shape. Model II (blue lines and points) relies on the assumption that $[Y_pZ]^{Z^{wt}}(\beta k_0)$ is a linear function (see Figure 1B). In this case $\beta k_0^{RB^+}([L])$ and $\beta k_0^{RB^-}([L])$ are proportional to $[Y_pZ]([L])$ of wild-type and *cheRcheB* cells, respectively (see Figure 1A and Figure 1C). The functional form of $[Y_pZ]^{Z^*}(\beta k_0)$ of CheZ mutant cells now has a concave shape (see Figure 1B). These two models are two extreme scenarios that both can explain the data shown in Figure 1A.

In the following sections we will also consider models that have less extreme functional forms for $[Y_pZ](\beta k_0)$; these models lie in between model I and model II. We construct such models, starting from models I and II, by defining functions $\beta k_0([L])$ as linear combinations $\alpha\ \beta k_0^{II}([L]) + (1-\alpha)\ \beta k_0^{I}([L])$, where α is a parameter between zero and one; for $\alpha = 0$ the model reduces to model I, while for $\alpha = 1$ the model reduces to model II. Model III (black lines and points) was constructed by putting α equal to 0.5. For this model, $[Y_pZ]^{Z^*}(\beta k_0)$ of CheZ mutant cells is slightly concave, whereas $[Y_pZ]^{Z^{wt}}(\beta k_0)$ of wild-type cells is slightly convex.

The model that can describe the response of $[Y_pZ]$ to changes in ligand concentration should not only be able to reproduce the dose-response curves of Figure 1, it should also satisfy other important conditions. Most importantly, wild-type cells can chemotax, which means that in their non-stimulated state they can respond to the addition as well as to the removal of attractant. Bacteria lacking $CheA_s$ are able to chemotax towards attractants as well, although less efficiently than wild-type bacteria [12]. These mutants are probably similar to CheZ mutants in that the binding of CheZ to the receptor cluster is hampered in both strains. The requirement that both strains can chemotax means that the concentration of $CheY_p$ in the non-stimulated state should be within the working range of the motor, i.e. between 1 and 5 μM [13,14].

Original model: The canonical push-pull network

We now address the question whether the canonical model for the chemotaxis pathway of *E. coli*, as given by Equations 1–3, can describe the experimental results of Vaknin and Berg [2]. We first study the effect of the spatial distribution of CheZ, thus leaving the other parameters unchanged. As we will show, the spatial distribution of CheZ alone is not sufficient to explain their experimental results. We will then also vary rate constants and concentrations to see whether the canonical model can describe these results.

To elucidate the effect of CheZ localization, we have computed the input-output relations for a network in which CheA and CheZ are colocalized at the receptor cluster (corresponding to wild-type cells) and for a network in which CheA is localized at the receptor cluster, while CheZ is distributed in the cytoplasm (corresponding to CheZ mutant cells); for both networks, the chemical reactions are given by Equations 1–3. The steady-state input-output relations of these networks were obtained numerically by discretizing the system on a 1D grid and propagating the chemical rate equations, which are given in the *Methods* section, in space and time until steady state was reached.

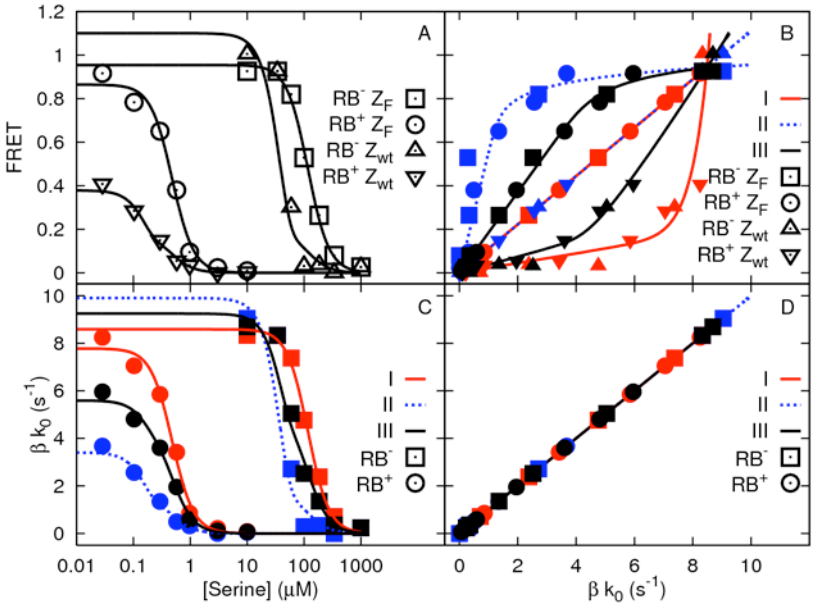

Figure 1. Three models that reproduce the response curves of Ref. [2]. A. The four response curves of Figure 5a in [2], rescaled according to Figure 1 of Text S1 and assuming a total concentration $[Z]_T = 1.1\mu M$. Model I (red data) is based on a linear dependence $\mathrm{FRET}(\beta k_0)$ for cells containing the non-localizing phosphatase mutant CheZ (see panel B). As a consequence, the activity of the receptor cluster in panel C is proportional to the FRET signal for CheZ mutant cells in panel A. The response $\mathrm{FRET}(\beta k_0)$ for cells containing wild-type CheZ is extremely sharp for model I (see panel B). Model II (blue data) is based on a linear function of $\mathrm{FRET}(\beta k_0)$ for cells with wild-type CheZ. As a consequence, $\beta k_0([L])$ is proportional to the dose-responses curve for cells with wild-type CheZ (compare panels A and C). In this case, the response curve $FRET(\beta k_0)$ for CheZ mutant cells is very concave. Model III was constructed by assuming that $\beta k_0([L])$ is a linear combination of the response functions of models I and II. The resulting response functions $\mathrm{FRET}(\beta k_0)$ in panel B are less extreme than those of models I and II. The straight line $\beta k_0(\beta k_0)$ in panel D helps to visualize the projection between panels B and C.
doi:10.1371/journal.pcbi.1000378.g001

As pointed out in the previous section, the input of the intracellular network is not directly the ligand concentration [L], but rather βk_0 (see Eq. 1), which implicitly depends upon [L]. Importantly, we first assume that the functional dependence of β on the ligand concentration [L], as well as the rate constants of all the reactions, is the same for wild-type and CheZ mutant cells: this allows us to elucidate the effect of colocalization of the antagonistic enzymes on the input-output relations. The model and the values of its parameters were taken from Sourjik and Berg [14].

The principal results of our calculations are shown in Figure 2. This figure shows for wild-type and CheZ mutant cells, the concentration of $\mathrm{CheY_pCheZ}$ (a $\mathrm{CheY_p}$ molecule bound to a CheZ dimer) and the concentration of $\mathrm{CheY_p}$ as a function of βk_0 (see Equation 1); the bullets correspond to the non-stimulated state of the network [14]. Figure 2 shows that the model predicts that the spatial distribution of CheZ affects the response to the addition of repellent or the removal of attractant, which corresponds to an increase in β. More importantly, the model predicts that the CheZ distribution should not affect the response to the addition of attractant: When βk_0 is lowered from its value $\beta^{\mathrm{ns}} k_0$ in the non-stimulated state, both the change in $[\mathrm{Y_p}]$ and $[\mathrm{Y_pZ}]$ do not depend much on the spatial distribution of CheZ. This result is thus in contrast with the drastic effect of enzyme localization on the response found by Vaknin and Berg [2].

The network given by Equations 1–3 is very similar to a canonical push-pull network, in which two enzymes covalently modify a substrate in an antagonistic manner [15] (see Text S2 for how these networks can be mapped onto each other). We have recently studied in detail the effect of enzyme localization on the response of a push-pull network [3]. Our principal finding is that enzyme localization *can* have a marked effect on the gain and sensitivity of push-pull networks, seemingly consistent with the experiments of Vaknin and Berg [2], but contradicting the numerical results shown in Figure 2. The resolution of this paradox is that both the quantitative and qualitative consequences of enzyme localization depend upon the regime in which the push-pull network operates. In particular, if the activation rate is independent of the substrate concentration and if the deactivation rate is linear in the messenger concentration, then phosphatase localization has no effect on the response curve [3]. This is precisely the case for the chemotaxis network studied here. For $\beta k_0 < \beta^{\mathrm{ns}} k_0$, CheZ is unsaturated [14] and the dephosphorylation rate of $\mathrm{CheY_p}$ is thus proportional to $[\mathrm{Y_p}]$. The influx J of $\mathrm{CheY_p}$ is constant, i.e. independent of [Y]. This is not because the phosphorylation reaction is in the zero-order regime; this reaction is, in fact, in the linear regime [14]. The influx J of $\mathrm{CheY_p}$ at the cell pole is constant because a) in steady state $J = k_3[\mathrm{A_pY}] = \beta k_0[\mathrm{A}]$ and b) in the weak activation regime CheA is predominantly unphosphorylated ($[\mathrm{A}] \approx [\mathrm{A}]_T$), which means that [A] is fairly insensitive to the spatial distribution of CheZ. Hence, according to the model of Equations 1–3, in this regime the concentration of $\mathrm{CheY_p}$ does not depend upon the spatial distribution of CheZ, which is indeed what Figure 2 shows.

However, while the model of Equations 1–3 predicts that in wild-type cells the response of $[\mathrm{Y_pZ}]$ to the addition of attractant does not depend on the location of CheZ, the experiments by Vaknin and Berg clearly demonstrate that it does [2]. What could be the origin of the discrepancy between the model predictions and the experimental results of Vaknin and Berg? As mentioned above, the response of $[\mathrm{Y_pZ}]$ to the ligand concentration [L] depends upon the response of $[\mathrm{Y_p}]$ to the activity of the receptor cluster, βk_0, and upon the response of βk_0 to the ligand

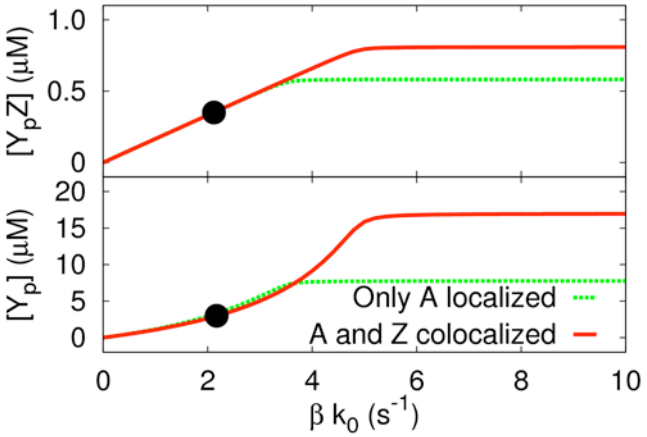

Figure 2. Total, integrated concentration of $CheY_p$ bound to CheZ, $\int_0^L [Y_pZ](x)dx$, and $CheY_p$, $\int_0^L [Y_p](x)dx$, as a function of βk_0 for the canonical model of the chemotaxis network of *E. coli*, shown in Equations 1–3. The red curves correspond to wild-type cells in which CheA and CheZ are colocalized at the receptor cluster, while the green curves correspond to the mutant cells in which CheA is localized at the pole, while CheZ freely diffuses in the cytoplasm. The bullets correspond to the non-stimulated state of the system. The diffusion constant of the diffusing components is $D = 5\mu m^2 s^{-1}$ [38]. For other parameter values, see [14].
doi:10.1371/journal.pcbi.1000378.g002

concentration [L]. If we keep with the assumption that the functional dependence of βk_0 on [L], $\beta k_0([L])$, is the same for both wild type and CheZ mutant cells, the discrepancy between the predictions of the canonical model and the experimental observations of Vaknin and Berg must lie in the dependence of $[Y_pZ]$ on βk_0. It is quite likely that the rate constants and/or concentrations that are used in the calculations differ from those *in vivo*. It is also possible that the topology of the canonical model of the intracellular chemotactic pathway, Eqs. 1–3, is incorrect. In order to discriminate between these two scenarios, we will, in the rest of this section, first address the question whether it is possible to explain the experimental observations with the canonical model by allowing for different values of parameters such as rate constants and protein concentrations. We will then argue that simply allowing for different parameter values is probably not sufficient to explain the experiments of Vaknin and Berg, and that thus the canonical model should be reconsidered.

Irrespective of the model parameters, it is always true that the rate of phosphorylation equals the rate of dephosphorylation if the system is in steady state. For the canonical model, i.e. Equations 1–3, this means that for both the spatially uniform network in which CheA and CheZ are colocalized, and the spatially non-uniform network in which CheZ is distributed in the cytoplasm, the following relation holds in steady state:

$$\beta k_0[A] = k_6[YpZ] \propto k_6 \mathrm{FRET}. \quad (4)$$

Here, "FRET" denotes the FRET signal, which is proportional to the total, integrated, concentration of $CheY_p$ bound to CheZ, $[Y_pZ]$. For the regime of interest, $\beta k_0 < \beta^{ns} k_0$, the concentration of unphosphorylated CheA, [A], is essentially constant for the conventional model, because only a small fraction of the total amount of CheA is phosphorylated; below we discuss scenarios in which this relation might not hold. Equation 4 thus shows that if $[A] \approx [A]_T$, the FRET signal only depends upon the activity of the receptor cluster, βk_0, and upon the phosphatase activity, k_6, but not upon other rate constants in the network, nor upon the expression levels of, for instance, CheY and CheZ. Moreover, if $[A] \approx [A]_T$, the FRET signal, in this model, is *linear* in the activity of the receptor cluster: $\mathrm{FRET} = c\,\beta([L])$, where $c = k_0[A]/k_6$ is the proportionality constant. Incidentally, this explains the linear dependence of $[Y_pZ]$ on βk_0 for $\beta k_0 < \beta k_0^{ns}$ in Figure 2B.

The linear relation between [YpZ] and βk_0 as predicted by the canonical model would mean that the dose-response curves, i.e. FRET([L]), solely reflect the response of the receptor cluster to the addition of ligand, $\beta k_0([L])$. Vaknin and Berg report the *renormalized* FRET response: they normalize the FRET signal at ligand concentration [L] to the FRET signal at zero ligand concentration, $[L] = 0$ [2]. If the response of $[Y_pZ]$ to βk_0 would indeed be linear, then the renormalized FRET signal would be given by $\mathrm{FRET}([L])/\mathrm{FRET}([L]=0) = \beta([L])/\beta([L]=0)$. Hence, the proportionality factor c would drop out. The renormalized FRET signal would thus be given by the dependence of the activity of the receptor cluster on the ligand concentration, $\beta k_0([L])$. While plotting the renormalized FRET signal may mask potentially useful information, this observation does allow us to draw an important conclusion: *If $\beta k_0([L])$ is the same for wild type and CheZ mutant cells, and as long as $[Y_pZ](\beta k_0)$ is linear, the canonical model cannot describe the experiments of Vaknin and Berg, even if we allow for different parameter values for the rate constants or protein concentrations.*

The experiments of Wang and Matsumura illustrate the importance of this conclusion [10]. Their experiments suggest that the phosphatase activity is enhanced by its interaction with $CheA_s$, which is localized at the receptor cluster [10]. This would predict that in the CheZ mutant cells (in which CheZ is distributed in the cytoplasm), the phosphatase activity is lower. This could either be due to a decrease in the CheZ-$CheY_p$ association rate k_4, or to a decrease in the catalytic activity k_6. Eq. 4 reveals that a change in the association rate k_4 has no effect on the FRET response curve, as long as $[A] \approx [A]_T$. In contrast, a change in k_6 would change the dependence of $[Y_pZ]$ on βk_0 (see Equation 4); in particular, decreasing k_6 would increase the slope. However, as long as the dependence of $[Y_pZ]$ on βk_0 is linear, the renormalized FRET response would still be given by $\beta k_0([L])$: merely changing the slope of $[Y_pZ]$ as a function βk_0 does not change the renormalized FRET response. More in general, only allowing for different rate constants or protein concentrations between the wild-type cells and mutant cells is not sufficient to explain the data, if indeed $\beta k_0([L])$ is the same for both cells and $[Y_pZ](\beta k_0)$ is linear.

The critical ingredient in the above analysis is that $[Y_pZ]$ varies linearly with βk_0, both for the wild-type and the CheZ mutant cells. We now first address the question whether deviations from this linear relation could explain the data, and then how these deviations might arise. The simplicity of the canonical model, Equations 1–3, does not allow for a convex dependence of $[Y_pZ]$ on βk_0. Figure 1B then immediately shows that any model that aims to describe the dose-response curves of both the wild-type cells and the CheZ mutant cells, should exhibit a linear relationship $[Y_pZ](\beta k_0)$ for wild-type cells and a concave function $[Y_pZ](\beta k_0)$ for CheZ mutant cells (blue data set). To generate a non-linear response of $[Y_pZ]$ as a function of βk_0 over the concentration range of interest, the condition $[A] \approx [A]_T$, which was the critical condition to generate a linear relationship (see Equation 4), should be violated; this means that $[A_p]$ should increase significantly within the concentration range of interest. An inspection of the canonical network, Equations 1–3, reveals that $[A_p]$ increases more rapidly with βk_0, when k_1, k_3, k_4 or k_6 decrease (k_2 and k_5 are very small, and can thus be neglected). The effect of changing these parameters can be understood by

considering the following relations in steady state: $k_6[\mathrm{Y_pZ}]=\beta k_0[\mathrm{A}]=k_3k_1[\mathrm{A_p}][\mathrm{Y}]/(k_2+k_3)$. For example, as k_6 decreases, $[\mathrm{Y_p}]$ and $[\mathrm{Y_pZ}]$ tend to increase, and $[\mathrm{Y}]$ tends to decrease; the latter means that to obey the above relations, $[\mathrm{A_p}]$ should increase. Decreasing k_6 thus means that $[\mathrm{Y_pZ}]$ as a function of βk_0 not only has a higher initial slope, but also levels off more rapidly because $[\mathrm{A_p}]$ increases: the function becomes concave for lower values of βk_0. Similarly, it can be deduced that while a decrease of k_1 does not change the initial slope of $[\mathrm{Y_pZ}](\beta k_0)$ (because for low βk_0, $[\mathrm{A}]=[\mathrm{A}]_\mathrm{T}$, and the slope is then independent of k_1 (see Equation 4)), it does lower the value of βk_0 at which $[\mathrm{A_p}]$ increases; again the function becomes concave for lower values of βk_0.

Changes in the rate constants (k_1, k_3, k_4, k_6) could thus potentially explain the dose-response curves measured by Vaknin and Berg [2]. We have tested by extensive numerical calculations, in which we did not only change these rate constants but also protein concentrations, whether changing these parameters can indeed explain the experiments. The results are shown in Text S2. The calculations reveal that changing k_1 and k_3 does not have a large effect (see Figures 4 and 5 of Text S2); moreover, it does not seem likely that changing CheZ affects the binding of CheY to CheA, although this cannot be ruled out. Changing k_4 and k_6 has a stronger effect: assuming that k_6 in the CheZ mutant cells is a factor 10 lower than k_6 in the wild-type cells yields a reasonable fit to the FRET data of Vaknin and Berg [2] (see Figure 7 of Text S2).

Do the CheZ mutant cells exhibit a tenfold lower phosphatase activity (k_6)? The canonical model with the assumption that in the CheZ mutant cells the phosphatase activity is ten times lower is an example of model I discussed in the previous section (blue lines in Figure 1B). While this model could explain the FRET data of Vaknin and Berg, it should be realized that according to this model the CheZ mutant cells would be tumbling all the time: as Figure 7 of Text S2 shows, in the non-stimulated state the concentration of $\mathrm{CheY_p}$ would be at its maximal value, and the clockwise bias would be close to unity. However, the experiments of Sanatinia *et al.* [12] show that both the wild-type and the mutant bacteria can chemotax, which suggests that not only in the wild-type cells, but also in the CheZ mutant cells, $[\mathrm{Y_p}]$ is within the working range of the motor when the cells are in their non-stimulated state. We therefore present two new models. In the next section, we consider a model of type I, in which the FRET signal in wild type cells is proportional to the activity of the receptor cluster βk_0, whereas the response curve $\mathrm{FRET}(\beta k_0)$ for mutant cells is strongly concave. In the subsequent section, we consider a model of type III that exhibits a weakly concave response curve $[\mathrm{Y_pZ}](\beta k_0)$ for the CheZ mutant cells, and, consequently, a convex response curve $[\mathrm{Y_pZ}](\beta k_0)$ for the wild-type cells.

The cooperative model

Recent experiments strongly suggest that the intracellular chemotaxis network of *E. coli* has a more complicated topology than that of the canonical push-pull network discussed in the previous section. In particular, in the canonical model discussed above the phosphatase reactions were described by simple Michaelis-Menten reactions. However, experiments of Eisenbach and coworkers [4,6] and Silversmith *et al.* [7] have shown that the activity of CheZ depends in a cooperative manner on the $\mathrm{CheY_p}$ concentration. It is clearly important to understand how the response curve $[\mathrm{Y_pZ}](\beta k_0)$ is affected by the cooperative dependence of phosphatase activity on $\mathrm{CheY_p}$ concentration. In this section, we present a simple model for the cooperative dependence of the phosphatase activity on $\mathrm{CheY_p}$ concentration, which can be solved analytically. Furthermore, we show that incorporation of cooperativity into the phosphatase reactions can lead to a model of type I (see Figure 1) and therefore gives a possible explanation for the experiments by Vaknin and Berg [2].

In vitro data [4,6,7] suggest that the activity of CheZ depends in a cooperative manner on the $\mathrm{CheY_p}$ concentration. The experiments of Eisenbach and coworkers [4,6] suggest that the activity of CheZ also depends in a cooperative manner on the CheZ concentration, suggesting that CheZ may oligomerize upon $\mathrm{CheY_p}$ binding [4–6]. Other biochemical *in vitro* experiments [16] and more recent *in vivo* FRET experiments [9], however, do not provide support for this idea. We therefore assume that the activity of CheZ in the mutant cells only depends cooperatively on the $\mathrm{CheY_p}$ concentration.

The model for the cooperative dephosphorylation of $\mathrm{CheY_p}$ by CheZ is based upon the following assumptions: 1) a single CheZ dimer can bind up to two $\mathrm{CheY_p}$ molecules; 2) CheZ can dephosphorylate $\mathrm{CheY_p}$ in both $\mathrm{CheY_p}$-bound states, thus dephosphorylation can occur when only a single $\mathrm{CheY_p}$ molecule is bound or when two $\mathrm{CheY_p}$ molecules are bound. This model can be described by two coupled Michaelis-Menten reactions, those of Eq. 3 in combination with

$$\mathrm{Y_pZ}+\mathrm{Y_p}\underset{k_8}{\overset{k_7}{\rightleftharpoons}}(\mathrm{Y_p})_2\mathrm{Z}\overset{k_9}{\rightarrow}\mathrm{Y}+\mathrm{Y_pZ} \tag{5}$$

In steady state, the phosphatase activity is given by

$$\frac{d[\mathrm{Y}]}{dt}=\frac{[\mathrm{Z}]_\mathrm{T}[\mathrm{Y_p}](k_6+k_9[\mathrm{Y_p}]/K_{\mathrm{M},2})}{K_{\mathrm{M},1}+[\mathrm{Y_p}]+[\mathrm{Y_p}]^2/K_{\mathrm{M},2}}, \tag{6}$$

where $[\mathrm{Z}]_\mathrm{T}$ is the total concentration of CheZ and $K_{\mathrm{M},1}=(k_5+k_6)/k_4$ and $K_{\mathrm{M},2}=(k_8+k_9)/k_7$ are the Michaelis-Menten constants of Equation 3 and Equation 5, respectively (see Text S3 for a derivation). It can be seen that if $k_9\gg k_6$ and if $K_{\mathrm{M},1}\gg K_{\mathrm{M},2}$, the dephosphorylation rate is given by

$$\frac{d[\mathrm{Y}]}{dt}=\frac{k_9[\mathrm{Z}]_\mathrm{T}[\mathrm{Y_p}]^2}{K_{\mathrm{M},1}K_{M,2}+[\mathrm{Y_p}]^2}. \tag{7}$$

This is a Hill function with a Hill coefficient of 2 and a concentration at which the rate is half maximal (the inflection point) given by $K_\mathrm{M}^\mathrm{eff}=\sqrt{K_{\mathrm{M},1}K_{\mathrm{M},2}}$. Clearly, strong cooperativity arises when 3) the binding of the first substrate molecule facilitates the binding of the second one, making $K_{\mathrm{M},1}\gg K_{\mathrm{M},2}$ and 4) the catalytic activity is higher when two substrate molecules are bound than when one is bound, i.e. $k_9\gg k_6$. In Text S3 we give an extended analysis of this model, which shows that it can fit the *in vitro* data of Blat and Eisenbach [6] not only qualitatively, but also quantitatively; this fit satisfies criteria 3) and 4). Recently, Silversmith *et al.* independently developed a similar model as that of Eqs. 3 and 5 on the basis of their *in vitro* experiments [7], although they did not present the analytical result of Eq. 6 [7]. Interestingly, their model also satisfies criterion 3): binding of the first $\mathrm{CheY_p}$ molecule facilitates the binding of the second $\mathrm{CheY_p}$ molecule. However, in their model binding of the second $\mathrm{CheY_p}$ molecule does not enhance the catalytic activity of CheZ [7], in contrast to our model. We cannot obtain a good fit to the *in vitro* data of Eisenbach and coworkers [6], nor, as discussed below, to the *in vivo* data of Vaknin and Berg [2], without relaxing criterion 4). Finally, we would like to emphasize that the rate constants

derived from fitting *in vivo* data may differ from those obtained from fitting *in vitro* data. In particular, diffusion-limited reaction rates will often be lower in living cells due to a lower diffusion constant, and a detailed analysis of this model (see Text S3) suggests that in this system this might be the case.

In the model presented in this section, we assume that in wild-type cells all CheZ proteins are localized at the receptor cluster, while in the CheZ mutant cells all CheZ proteins freely diffusive in the cytoplasm. For both cells, the chemical reactions are given by Eqs. 1–3 and Eq. 5. However, while the rate constants of the phosphorylation reactions in Eqs. 1 and 2 are identical for both cells, they differ for the dephosphorylation reactions of Eqs. 3 and 5. In particular, in order to obtain a good fit to the FRET data [2], we have to assume that in the CheZ mutant cells CheZ acts cooperatively, while in the wild-type cells CheZ acts non-cooperatively. Specifically, while for the wild-type cells, not only the two $CheY_p$-CheZ association rates k_4 and k_7, but also the two catalytic activities k_6 and k_9 can be assumed to be identical—$k_4=k_7$; $k_6=k_9$—, for the CheZ mutant cells it is required that $k_4<k_7$ and $k_6<k_9$ (see caption of Figure 3 for parameter values).

The results for this model are shown in Figure 3. The FRET response of wild-type cells is similar to that in the canonical model discussed in the previous section; it is essentially linear in βk_0 over the relevant range of βk_0, because CheZ acts non-cooperatively. However, the FRET response of wild-type cells is weaker than that of CheZ mutant cells over this range. This is because the catalytic activity of CheZ with one $CheY_p$ molecule bound, k_6, is higher in wild-type cells than in CheZ mutant cells. Indeed, this model would suggest that the interaction of CheA with CheZ enhances the catalytic activity of CheZ when one $CheY_p$ molecule is bound to CheZ. Another important point to note is that the FRET response of CheZ mutant cells is strongly concave over the relevant range of βk_0. This model is indeed an example of type I, as discussed in the section *Decomposing the response*. The concave FRET response of CheZ mutant cells is a consequence of the cooperative dephosphorylation of $CheY_p$ by CheZ: for small receptor activities βk_0, $[Y_p]$ is low, CheZ is mostly singly occupied by $CheY_p$, and since the catalytic activity of $CheY_pCheZ$, k_6, is relatively small (as compared to that of $(CheY_p)_2CheZ$, k_9), a given increase in βk_0 must be balanced by a relatively large increase in $[Y_pZ]$ and hence the FRET signal; for higher βk_0, $[Y_p]$ increases, CheZ becomes doubly occupied with $CheY_p$, and since $(CheY_p)_2CheZ$ has a higher catalytic activity than $CheY_pCheZ$, a given increase in receptor activity βk_0 is balanced by a relatively small increase in $[(Y_p)_2Z]$. Indeed, if k_9 would be similar to k_6, as Silversmith *et al.* propose [7], the FRET response of the CheZ mutant cells would not be concave, and no good fit to the data of Vaknin and Berg [2] could be obtained.

Differential affinity and catalytic activity of CheZ

While the model discussed in the previous section can describe the FRET response as measured by Vaknin and Berg [2], it also assumes that in wild-type cells all CheZ proteins are localized at the receptor cluster. However, the data of Vaknin and Berg [2] suggest that only a small fraction of CheZ is localized at the receptor cluster. We therefore present here an alternative model, which, in our opinion, is consistent with the currently available experimental data.

The Model. The key ingredients of our model are:

1. *In wild-type cells, a small fraction of CheZ, of 10–20%, is bound to the receptor cluster, while the remainder diffuses freely through the cytoplasm.* Figure 2b of Vaknin and Berg [2] shows the cyan signal, coming from CFP fused to CheZ, *after the addition of attractant.* This signal represents the spatial distribution of CheZ. The figure suggests that about 10–20% of CheZ is bound to the receptor cluster, with the remainder more or less homogeneously distributed in the cytoplasm. This estimate is consistent with that based on the known chemistry of CheZ binding to the receptor cluster. CheZ can be localized to the receptor cluster via binding to CheA, which is part of the receptor cluster. CheA exists in two forms, $CheA_s$ and $CheA_L$, which can form the following dimers: $CheA_LCheA_L$, $CheA_LCheA_s$, and $CheA_LCheA_s$. The first two, $CheA_LCheA_L$ and $CheA_LCheA_s$, have catalytic activity and can transfer phosphoryl groups to CheY [17–20]; the third, the homodimer $CheA_sCheA_s$, does not have catalytic activity, but can bind CheZ. Earlier experiments suggest that CheZ binds selectively to $CheA_s$ [8,10,21], although recent FRET experiments indicate that CheZ also binds to $CheA_L$ [9]. Following Lipkow [11], we estimate that the number of $CheA_sCheA_s$ homodimers is about 360, while the number of CheZ dimers is about 1600 [22]. If we assume that CheZ predominantly binds $CheA_sCheA_s$, and that each of the $CheA_sCheA_s$ homodimers strongly binds one CheZ dimer, we arrive at the estimate that about 20% of the CheZ dimers is bound to the cluster, consistent with the estimate based on the FRET data of Vaknin and Berg [2].
2. *In wild-type cells, $CheY_p$ has a much higher affinity for CheZ bound to CheA than for CheZ freely diffusing in the cytoplasm.* Figure 3a of Vaknin and Berg [2] shows that in non-stimulated cells containing wild-type CheZ, the total amount of $[Y_pZ]$ in the

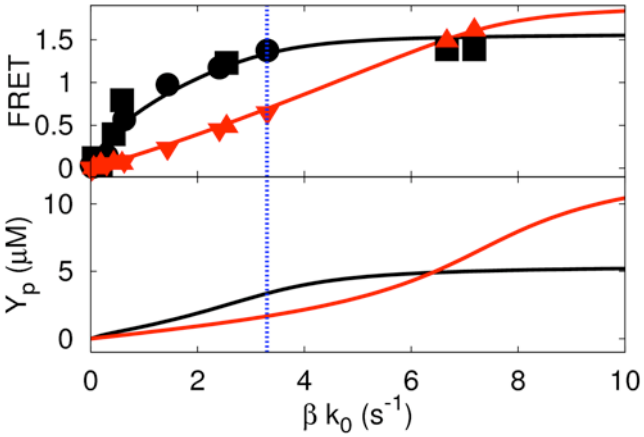

Figure 3. FRET vs. βk_0 and $[Y_p]$ vs. βk_0 for the best fit of the cooperative model (Equations 1–3 and 5). In this model, with $\alpha=0.9$ (see Figure 1), it is assumed that in wild-type cells all CheZ proteins are bound to the receptor cluster, while in the CheZ mutant cells all CheZ proteins diffusive in the cytoplasm. The chemical reactions of this model are given by Eqs. 1–3 and Eq. 5, for both cells. The black line and symbols correspond to CheZ mutant cells, while the red line and symbols correspond to wild type cells. The dotted vertical line denotes the value of βk_0 in the non-stimulated state. The FRET signal is assumed to be proportional to $[Y_pZ]+2[(Y_p)_2Z]$. The smaller concentration of $CheY_p$ in mutant cells when βk_0 is large is due to the fact that in these cells, CheZ diffuses (see also Ref. [3]). The values of the rate constants that are the same for wild-type and CheZ mutant cells are: $k_1=3\cdot10^6M^{-1}s^{-1}$, $k_3=750\ s^{-1}$, $k_7=1\cdot10^7M^{-1}s^{-1}$, $k_9=30\ s^{-1}$; the values of the rate constants that are different between wild-type and CheZ mutant cells are: $k_4=1\cdot10^7M^{-1}s^{-1}$ for wild type cells and $k_4=2\cdot10^6M^{-1}s^{-1}$ for mutant cells, $k_6=30\ s^{-1}$ for wild type cells and $k_6=2\ s^{-1}$ for mutant cells. The total concentrations are $[Y]_T=17.9\ \mu M$, $[Z]_T=1.1\ \mu M$ and $[A]_T=5\ \mu M$ (for parameter values, see [6,14,39]). The diffusion coefficient of all cytosolic components is set to 5 $\mu m^2\ s^{-1}$; all enzyme-substrate dissociation rates are zero.
doi:10.1371/journal.pcbi.1000378.g003

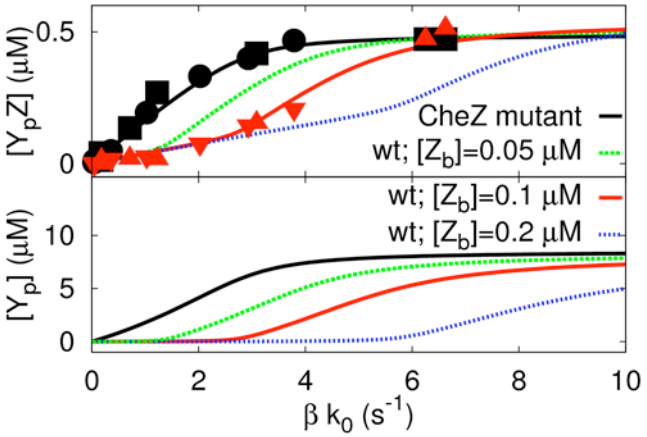

Figure 4. The effect of the total amount of CheZ that is bound to the cluster, as given by $[Z_b]_T$, on the response of $[Y_pZ]$ and $[Y_p]$ in the differential-affinity-and-catalytic-activity model (Equations 1–3 and Equation 8). The black line corresponds to the prediction of our model for CheZ mutant cells, while the red line corresponds to the model prediction for wild-type cells, in which $[Z_b]_T = 0.1\ \mu$M. The green and blue dashed lines correspond to the model prediction for wild-type cells with $[Z_b]_T = 0.05\ \mu$M and 0.2 μM, respectively. The symbols correspond to the experimental data of Vaknin and Berg [2]. The circles correspond to CheZ mutant cells with CheR and CheB, the squares correspond to CheZ mutant cells without CheR and CheB, the triangles correspond to wild-type cells and the inverted triangles correspond to wild-type cells without CheR and CheB. Please note that as $[Z_b]_T$ is increased, the inflection point that separates the first from the second regime shifts to higher values of βk_0 and to higher values of $[Y_pZ]$—to a good approximation, at this point $[Y_pZ] \approx [Z_b]_T$. It is also seen that $CheY_p$ in the first regime is essentially zero. This is because the phosphatase activity of CheZ at the receptor cluster is much higher than that of CheZ in the cytoplasm. The baseline parameters are: $k_1 = 3{\cdot}10^6\ M^{-1}s^{-1}$, $k_3 = 750\ s^{-1}$, $k_4 = 3{\cdot}10^6 M^{-1}s^{-1}$, $k_6 = 30\ s^{-1}$, $k_{10} = 3{\cdot}10^9 M^{-1}s^{-1}$, $k_{12} = 130\ s^{-1}$, $[Y]_T = 17.9\ \mu$M, $[Z]_T = 1\ \mu$M, $[Z_b] = 0.1\ \mu$M and $[A]_T = 5\ \mu M$ (for parameter values, see [14,39]). The diffusion coefficient of all cytosolic components is 5 $\mu m^2\ s^{-1}$; all enzyme-substrate dissociation rates were set to zero.
doi:10.1371/journal.pcbi.1000378.g004

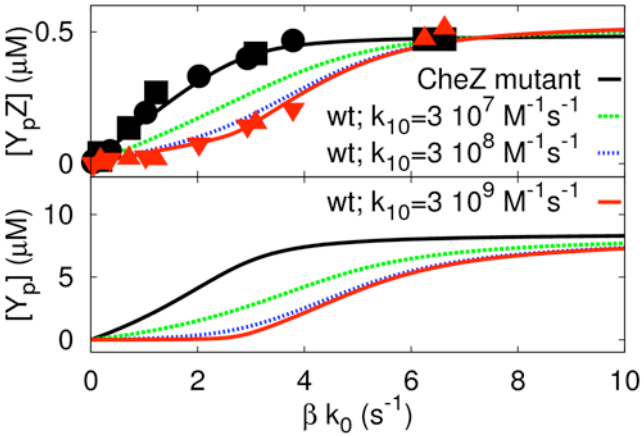

Figure 5. The effect of the rate of association between $CheY_p$ and CheZ bound to the receptor cluster, k_{10}, on the response of $[Y_pZ]$ and $[Y_p]$ in the differential-affinity-and-catalytic-activity model (Equations 1–3 and Equation 8). The black line and black symbols corresponds to the CheZ mutant cells (see also Figure 4), while the red line and red symbols correspond to cells containing wild-type CheZ, in which $k_{10} = 3{\cdot}10^9 M^{-1}s^{-1}$; the dashed green and blue lines correspond to CheZ-wild-type cells with $k_{10} = 3{\cdot}10^7 M^{-1}s^{-1}$ and $k_{10} = 3{\cdot}10^8 M^{-1}s^{-1}$, respectively. Please note that as k_{10} is lowered, the distinction between the two regimes becomes less sharp, because more $CheY_p$ molecules diffuse into the cytoplasm before they will bind CheZ molecules. For parameter values, see the caption of Figure 4.
doi:10.1371/journal.pcbi.1000378.g005

cytoplasm roughly equals that of $[Y_pZ]$ at the receptor cluster; yet, as mentioned above, Figure 2b of Ref. [2] shows that the total amount of CheZ at the cluster is about 10–20% of that in the cytoplasm; this means that CheZ bound to CheA at the receptor cluster has a higher affinity for $CheY_p$ than CheZ in the cytoplasm, as can also be seen directly from Figure 2d of Ref. [2]. The higher affinity could be due to a lower enzyme-substrate dissociation rate, or a higher enzyme-substrate association rate. We assume that binding of CheZ to CheA increases the association rate. It is conceivable that CheA enhances the CheZ- $CheY_p$ association rate in a manner analogous to the gain of function mutations in CheZ studied by Silversmith *et al.* [7]: CheA might relieve inhibition of the binding of $CheY_p$ to CheZ. A more speculative hypothesis is that CheA increases the CheZ- $CheY_p$ association rate because of the close physical proximity between CheA, where CheY is phosphorylated, and cluster-bound CheZ: a CheY molecule that has just been phosphorylated by a $CheA_p$ dimer at the cluster, can very rapidly bind cluster-bound CheZ; in fact, if $CheY_p$ would be directly transferred from $CheA_p$ to CheZ, the association rate could even exceed the diffusion-limited rate.

3. *In wild-type cells, CheZ bound to CheA at the receptor cluster has a higher phosphatase activity than CheZ in the cytoplasm.* The experiments of Wang and Matsumura [10] suggest that the interaction of CheZ with CheA enhances its dephosphorylating activity. This could either be due to a higher CheZ-$CheY_p$ association rate, or to a higher catalytic activity. We assume that binding of CheZ to CheA not only increases the CheZ-$CheY_p$ association rate, as discussed above, but also the catalytic activity of CheZ.
4. *In CheZ mutant cells, CheZ cannot bind to CheA at the cluster. CheZ in these cells has the same phosphatase activity and the same binding affinity for $CheY_p$ as CheZ in wild-type cells that is not bound to CheA at the cluster.* As crystallographic data [23] and mutagenesis data [20] suggest, we assume that in the CheZ mutant protein only the domain that allows it to interact with CheA is affected; the part that allows the CheZ mutant protein to interact with $CheY_p$ is thus assumed to be unaffected. This assumption is not critical for obtaining a good fit of our model to the data of Vaknin and Berg [2]. It is merely a simplifying assumption to reduce the number of free parameters. Indeed, it would be of interest to characterize the enzymatic activity of CheZ F98S—the CheZ mutant used by Vaknin and Berg [2]—since experiments by Silversmith *et al.* show that mutations far from the active site can, in fact, significantly change the enzymatic activity of CheZ [7].

For reasons of clarity, we first disregard the cooperativity in the phosphatase activity of CheZ. The CheZ mutant cells are thus described by the reactions of Eqs. 1–3, while the wild-type cells are described by the reactions of Eqs. 1–2, Eq. 3 for the reactions involving diffusive CheZ and the following reactions involving localized CheZ:

$$Y_p + Z_b \underset{k_{11}}{\overset{k_{10}}{\rightleftharpoons}} Y_pZ_b \overset{k_{12}}{\rightarrow} Y + Z_b \qquad (8)$$

Here, the total concentration of localized CheZ, $[Z_b]_T = [Z_b] + [Y_pZ_b]$, is low as compared to the total concentration of CheZ, $[Z]_T$. Furthermore, the association rate k_{10} and the catalytic activity k_{12} of localized CheZ, are high as compared to

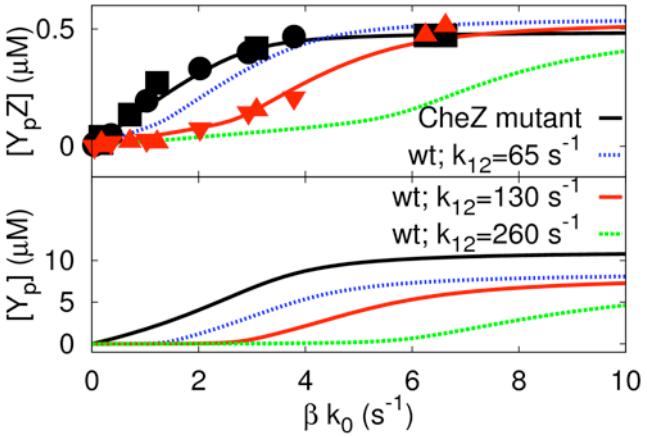

Figure 6. The effect of the catalytic rate of CheZ bound to the receptor cluster, k_{12}, on the response of $[Y_pZ]$ and $[Y_p]$ in the differential-affinity-and-catalytic-activity model (Equations 1–3 and Equation 8). The black line and black symbols corresponds to the CheZ mutant cells (see also Figure 4), while the red line and red symbols correspond to CheZ-wild-type cells, in which $k_{12}=130\text{s}^{-1}$; the dashed green and blue lines correspond to CheZ-wild-type cells with $k_{12}=65$ and $k_{12}=260\text{s}^{-1}$, respectively. Please note that as k_{12} is increased, the initial slope of $[Y_pZ](\beta k_0)$ of wild-type cells, which is inversely proportional to k_{12}, is decreased; the slope of the second regime is, to a good approximation, inversely proportional to the catalytic activity of freely diffusive CheZ, k_6, and thus fairly constant. Please also note that since the height of the inflection point is given by $[Y_pZ]\approx[Z_b]_T$ and thus independent of k_{12}, the inflection point shifts to higher values of βk_0 with increasing k_{12}.
doi:10.1371/journal.pcbi.1000378.g006

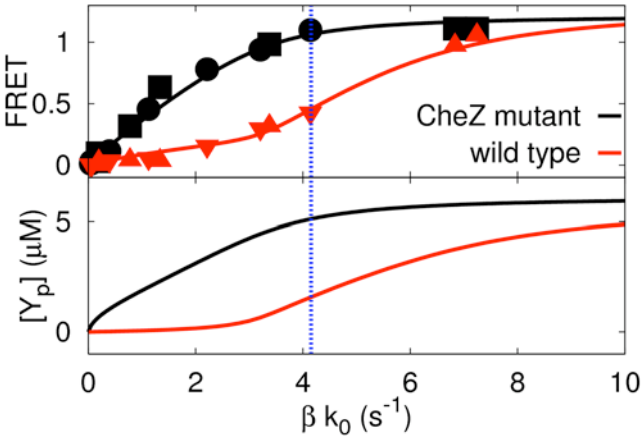

Figure 7. FRET vs. βk_0 and $[Y_p]$ vs. βk_0 for the best fit of the full differential-affinity-and-catalytic-activity model, which includes cooperativity in CheZ (Equations 1–3, and Equations 5, 8 and 9). The black line and symbols correspond to CheZ mutant cells, while the red line and symbols correspond to cells containing wild-type CheZ (see also Figure 4). The FRET signal is assumed to be proportional to $[Y_pZ]+2[(Y_p)_2Z]+[Y_pZ_b]+2[(Y_p)_2Z_b]$; the value of $\alpha=0.75$ (see Figure 1). The dotted vertical line denotes the value of βk_0 in the non-stimulated state. The parameter values are $k_1=3\cdot10^6\text{M}^{-1}\text{s}^{-1}$, $k_3=750\ \text{s}^{-1}$, $k_4=3.6\cdot10^5\text{M}^{-1}\text{s}^{-1}$, $k_6=7.5\ \text{s}^{-1}$, $k_{10}=6\cdot10^8\text{M}^{-1}\text{s}^{-1}$, $k_{12}=40\ \text{s}^{-1}$, $k_7=3\cdot10^7\text{M}^{-1}\text{s}^{-1}$, $k_9=30\ \text{s}^{-1}$, $k_{13}=9\cdot10^8\text{M}^{-1}\text{s}^{-1}$, $k_{15}=160\ \text{s}^{-1}$; $[Y]_T=17.9\ \mu\text{M}$, $[Z]_T=1\ \mu\text{M}$, $[Z_b]_T=0.1\ \mu\text{M}$ and $[A]_T=5\ \mu\text{M}$ (for parameter values, see [6,14,39]). The diffusion coefficient of all cytosolic components is set to 5 $\mu\text{m}^2\ \text{s}^{-1}$; all enzyme-substrate dissociation rates are zero.
doi:10.1371/journal.pcbi.1000378.g007

the corresponding rates k_4 and k_6 for diffusive CheZ. As we will show below, the critical parameters of this model are the fraction of CheZ bound to CheA at the receptor cluster, the ratio of the association rates $k_{10}:k_4$ and the ratio of the catalytic activities $k_{12}:k_6$.

The model presented here is similar to that of Lipkow [11] in that both assume that part of CheZ can bind the cluster. However, the models also differ in two important aspects: 1) in the model of Lipkow [11], the binding of CheZ to CheA is conditional on the binding of CheZ to $CheY_p$; consequently, while in our model the bound fraction of CheZ is fairly constant in time, in the model of Lipkow [11] the amount of CheZ bound to the cluster depends upon the current stimulus level: for instance, in her model, after the removal of attractant, CheZ moves from the cytoplasm to the cluster upon binding of $CheY_p$; 2) in the model of Lipkow [11], the binding of one $CheY_pCheZ$ pair to a CheA homodimer, can nucleate the formation of oligomers of $CheY_pCheZ$ pairs at the cluster. However, as mentioned above, recent *in vitro* [7,16] and *in vivo* experiments [9] seem to disprove the idea of CheZ oligomerization. Our calculations reveal that CheZ oligomerization is not necessary; the conditions listed above, are sufficient to explain the FRET data of Vaknin and Berg [2]. Moreover, the relative simplicity of our model makes it possible to elucidate the mechanism by which differential enzyme-substrate binding affinity and differential catalytic activity can sharpen the response curve.

Figures 4–6 show how the total amount of $CheY_pCheZ$ pairs and $CheY_p$ is affected by varying the critical parameters in this model: the fraction of CheZ bound to the cluster (Figure 4), the rate k_{10} at which $CheY_p$ associates with CheZ at the cluster (Figure 5), and the catalytic rate k_{12} of CheZ at the cluster (Figure 6); the baseline parameters are given in Figure 4. In all figures, the black line corresponds to CheZ mutant cells; the red line corresponds to CheZ wild-type cells with the baseline parameter set; the green and blue lines correspond to the results of the CheZ wild-type cells, where the parameter of interest is either increased or decreased (see caption for parameter values). The black and red symbols correspond to the experimental results of Vaknin and Berg [2], as described in section *Decomposing the response*; the value of α was, somewhat arbitrarily, taken to be $\alpha=0.65$, which means that $[Y_pZ](\beta k_0)$ is sigmoidal for CheZ wild-type cells and hyperbolic for CheZ mutant cells. The origin of the hyperbolic curve of the CheZ mutant cells is similar to that which underlies the response curves of the canonical model: $[Y_pZ]\propto\beta k_0[A]$, where initially, as βk_0 increases from zero, $[A]\approx[A]_T$ is constant but then decreases as $[A_p]$ increases significantly (see section *Original Model*). We will now discuss the origin of the sigmoidal curves of $[Y_pZ](\beta k_0)$ of the wild-type cells.

Figures 4–6 show that the response curves of $[Y_pZ](\beta k_0)$ of wild-type cells effectively consist of two parts, corresponding to the binding of $CheY_p$ to cluster-bound CheZ and freely diffusive CheZ, respectively. When βk_0 is low, a CheY molecule that has just been phosphorylated by a CheA dimer at the cluster, will most likely bind a CheZ dimer that is bound to the cluster because of the higher association rate between $CheY_p$ and cluster-bound CheZ, as compared to that between $CheY_p$ and freely diffusive CheZ: $k_{10}>k_4$. Since cluster-bound CheZ has a high phosphatase activity, the concentration of $CheY_p$ and hence $CheY_p$ bound to CheZ will initially increase only slowly with βk_0. Nevertheless, at some point CheZ at the cluster will become saturated with $CheY_p$. At this point $[Y_pZ]\approx[Z_b]_T$. When βk_0 is then increased further, a phosphorylated CheY molecule can no longer bind a cluster-bound CheZ dimer. It will then diffuse into the cytoplasm, where it can bind freely diffusive CheZ. Since the catalytic activity of CheZ in the cytoplasm is lower than that of CheZ bound to CheA at the

cluster, $[Y_pZ]$ and $[Y_p]$ will now quickly rise. This combination of differential affinity and differential catalytic activity thus provides a generic mechanism for enhancing the sharpness of the response.

We can now understand the effect of varying the critical parameters in this model. As the fraction of CheZ that is bound to the cluster increases (from green to red to blue in Figure 4), the amount of $CheY_p$ needed to saturate cluster-bound CheZ increases, leading to a shift of the inflection point in $[Y_pZ](\beta k_0)$ to higher values of βk_0. However, while increasing the fraction of cluster-bound CheZ shifts the inflection point to higher values of βk_0, it does not significantly change the initial slope of $[Y_pZ](\beta k_0)$, nor does it change the slope $[Y_pZ](\beta k_0)$ after the inflection point: these slopes are determined by the catalytic activities of cluster-bound CheZ and freely diffusive CheZ, k_{12} and k_6, respectively. This can be seen in Figure 6: as the catalytic activity of k_{12} is increased (from blue to red to green), the initial slope of $[Y_pZ](\beta k_0)$ decreases. Please also note that since the slope of $[Y_pZ](\beta k_0)$ after the inflection point is determined by parameters of freely diffusive CheZ, it is similar to the initial slope of $[Y_pZ](\beta k_0)$ of the CheZ mutant cells, which indeed only contain freely diffusive CheZ, exhibiting the same phosphatase activity as diffusive CheZ in wild-type cells. Figure 5 illustrates the importance of the association rate. As the rate of association between $CheY_p$ and cluster-bound CheZ decreases (from red to blue to green), the response curve $[Y_pZ](\beta k_0)$ of CheZ cells moves towards that of the CheZ mutant cells. The reason is that as the rate of association between $CheY_p$ and cluster-bound CheZ is lowered, it becomes more likely that a phosphorylated CheY molecule diffuses into the cytoplasm, where it will be dephosphorylated by freely diffusive CheZ with a lower catalytic activity.

The differential-affinity-and-activity model is able to explain the measured difference between the response curves for the CheZ mutant cells and the CheZ wild-type cells. However, while the response curves of Vaknin and Berg [2] can be reproduced by the model, this is not the only constraint. As discussed above, both wild-type and CheZ mutant cells should be able to chemotax [12]. This means that the model should give $CheY_p$ concentrations between 1 and 5 μM for both strains in the non-stimulated state [14]. As can be seen from the fit used in Figures 4–6, in the CheZ mutant, the $CheY_p$ concentration is 8 μM in the non-stimulated state, which is well outside this range.

This fit can, however, be improved by taking into account the effect of cooperativity in the phosphatase reactions, which we have neglected thus far in the differential-affinity-and-activity model. The reactions of diffusive CheZ, both in the wild-type cells and in the CheZ mutants cells, are given by Eqs. 3 and 5, while the reactions involving CheZ localized at the receptor cluster in wild-type cells are given by Eq. 8 in combination with

$$Y_pZ_b + Y_p \underset{k_{14}}{\overset{k_{13}}{\rightleftharpoons}} (Y_p)_2Z_b \overset{k_{15}}{\rightarrow} Y + Y_pZ_b \qquad (9)$$

As before, we assume that both the affinity to $CheY_p$ and the phosphatase activity of CheZ are enhanced when CheZ is localized to CheA at the receptor cluster. This means that the association rates k_{10} and k_{13} are much larger than the corresponding association rates for cytosolic CheZ, and that the catalytic activity k_{15} is larger than the catalytic activity k_9 for cytosolic CheZ.

Figure 7 shows $[Y_pZ](\beta k_0)$ and $[Y_p](\beta k_0)$ for CheZ wild-type cells and CheZ mutant cells [2]. In combination with a response curve for βk_0 vs. [Serine] with $\alpha = 0.75$, the four dose-response curves in Figures 5a and 5c of Ref. [2] are reproduced. Comparing Figure 7 with Figures 4–6 of the simplified differential-affinity-and-activity model shows that the cooperative dependence of the phosphatase activity on $CheY_p$ concentration does not dramatically affect the dose-response curves, a conclusion that was also reached by Sourjik and Berg [14]. Indeed, in this model it is possible to obtain a good fit to the data [2] while assuming that the catalytic activity of CheZ is independent of the number of bound $CheY_p$ molecules, as suggested by the *in vitro* observations of Silversmith *et al.* [7] (data not shown); the critical ingredients of this model are that the binding affinity and catalytic activity of cluster-bound CheZ are higher than those of freely diffusive CheZ. As for the model without CheZ cooperativity, $[Y_pZ](\beta k_0)$ is in agreement with experiment, both for CheZ wild-type and CheZ mutant cells. Moreover, the $[Y_p](\beta k_0)$ response curve of the CheZ wild-type cells agrees with experiment in the sense that the concentration of $CheY_p$ equals 2 μM in the non-stimulated state, which is within the working range of the motor. The concentration of $CheY_p$ in the CheZ mutant cells in their non-stimulated state is around 5 μM, which is lower than that in the simplified differential-affinity-and-activity model, but still at the high end of the working range of the motor.

Discussion

A new model for the intracellular signaling network

The experiments by Vaknin and Berg on the effect of CheZ localization on the dose-response curves of *E. coli* [2] impose strong constraints on the design of a model of the intracellular chemotaxis network. These experiments unambiguously demonstrate that the second derivative of $[Y_pZ](\beta k_0)$ of CheZ wild-type cells is larger than that of CheZ mutant cells (see Figure 1). The topology of the intracellular chemotaxis network of the canonical model (Equations 1–3) is such that the second derivative of $[Y_pZ](\beta k_0)$ must be equal to or smaller than zero: according to the canonical model the response curve cannot be convex. One way to fit the data is to assume that the response curve $[Y_pZ](\beta k_0)$ of CheZ wild-type cells is a straight line over the concentration range of interest, while $[Y_pZ](\beta k_0)$ of CheZ mutant cells is concave. The canonical model can yield such response curves. However, this scenario requires that in the CheZ mutant cells, some of the rate constants, such as the phosphatase activity, differ strongly from those in wild-type cells. Moreover, this would mean that CheZ mutant cells would adapt to a state in which $[Y_p]$ is outside the working range of the motor. This scenario thus seems unlikely, although it cannot be ruled out.

Here, we have presented two different models that can explain the FRET data of Vaknin and Berg [2]. In the first model, $[Y_pZ](\beta k_0)$ of CheZ wild-type cells is linear, while $[Y_pZ](\beta k_0)$ of CheZ mutant cells is strongly concave. The model is based on the *in vitro* observation that CheZ dephosphorylates $CheY_p$ in a cooperative manner [5–7]. The model leads over the relevant range of interest to fairly similar response curves $[Y_p](\beta k_0)$ for wild-type and mutant cells, and the non-stimulated state lies around 3 μM. This model, however, assumes that in wild-type cells all CheZ proteins are localized at the receptor cluster, while the data of Vaknin and Berg [2] suggest that in these cells only a fraction of about 10–20% is localized at the receptor cluster.

We have therefore presented an alternative model that is consistent with most, if not all, of the currently available data. In this model, $[Y_pZ](\beta k_0)$ of CheZ wild-type cells is sigmoidal, while $[Y_pZ](\beta k_0)$ of CheZ mutant cells is hyperbolic. The model relies on the assumption that a small fraction of CheZ is localized at the receptor cluster, while the remainder freely diffuses in the cytoplasm; moreover, it assumes that CheZ localized at the receptor cluster has both a higher binding affinity for $CheY_p$ and a

higher catalytic activity than CheZ in the cytoplasm. All these assumptions seem to be supported by experiment [2,10].

In essence, the model that we propose consists of a push-pull network with one activating enzyme, CheA, and two deactivating enzymes, CheZ bound to the cluster and CheZ that freely diffuses in the cytoplasm. Our analysis shows that the competition between these two deactivating enzymes for binding and deactivating the substrate can yield an ultrasensitive response even when the push-pull network does not operate in the zero-order regime. In fact, this mechanism of differential-affinity-and-catalytic-activity is evocative of the "branch point effect", in which the interdependence of the activities of two branch-point enzymes that compete for a common substrate can yield an abrupt change in the flux through one of the enzymes [24]. In the model proposed here, the spatial dependence of both the substrate-binding affinity and catalytic activity of CheZ only acts to create two types of deactivating enzymes; the proposed scheme could also work in a well-stirred model if one assumes that there exist two deactivating-enzyme species.

Does the intracellular signaling pathway contribute to the gain?

If the response function $[Y_pZ](\beta k_0)$ of wild-type cells is sigmoidal, as the differential-affinity-and-catalytic-activity model predicts, then the large number of recent studies on signal amplification by the receptor cluster has to be reconsidered [25–33]. If the relation between $[Y_pZ]$ and βk_0 would be linear, as predicted for wild-type cells in the canonical and cooperative model, then the renormalized FRET response would be given by the dependence of the activity of the receptor cluster, βk_0, on the ligand concentration [L]. This would justify the studies that describe the 'front end' amplification of the chemotaxis network, namely the response of $[Y_pZ]$ to changes in [L], in terms of the signal amplification properties of the receptor cluster [25–33]. However, if the dependence of $[Y_pZ]$ on the activity of the receptor cluster, βk_0, would not be linear, then the front end amplification would not be fully determined by the response of the receptor cluster to changes in the ligand concentration. Indeed, to explain the front-end gain, the extent to which the signal is amplified as it is transmitted from the receptor cluster to $CheY_pCheZ$ would then also have to be taken into account.

Recently, Kim *et al.* experimentally addressed the question whether CheZ contributes to the gain of the chemotaxis network [34]. To this end, they compared the motor response of wild-type cells to that of Δ*cheZ* mutant cells in which the activity of the receptor cluster was adjusted by mutating the Tsr receptor to compensate for the change in $CheY_p$ levels [34]. They observed that the change in the motor bias upon a change in ligand concentration was similar for these cells, and concluded that CheZ does not contribute to the gain. However, it should be noted that the mutations in the Tsr receptor as made by Kim *et al.* [34] may affect the signal amplification by the receptor cluster, especially since it is believed that interactions between receptors (and even between receptors of different types) strongly affect the gain [25–33]. If this would be the case, then the observation that in the "bias adjusted" Δ*cheZ* mutant cells the motor response is similar to that of wild-type cells, would imply that CheZ does contribute to the gain. Our analysis supports a scenario in which CheZ contributes to the gain, but cannot rule out the alternative scenario. If CheZ does not contribute to the gain, then $[Y_p](\beta k_0)$ should be the same for wild-type cells and CheZ mutant cells over the relevant range of the activity of the receptor cluster. In our differential-affinity-and-catalytic-activity model, which is consistent with most of the experimental data, the response curves are different (Figure 7), but in our cooperative model they are, in fact, fairly similar (Figure 3). The problem is that while the data of Vaknin and Berg [2] put strong constraints on any model that aims to describe the response of the intracellular signaling pathway, they do not uniquely prescribe it (Figure 1). To elucidate the response of the intracellular signaling pathway and to discriminate between the models that we propose, we believe that FRET measurements should be made of $CheY_p$-CheZ and $CheY_p$-FLiM interactions [9], not only for wild-type cells, but also for Δ*cheZ* mutants [34] and the CheZ F98S mutants studied by Vaknin and Berg [2].

The concentration of $CheY_p$ in non-stimulated cells

While the differential-affinity-and-catalytic-activity model can describe the dose-response curves as reported by Vaknin and Berg [2], a number of issues remain. The first is that in the full differential-affinity-and-catalytic-activity model, which takes into account CheZ cooperativity, the *total* concentration of $[Y_p]$ in non-stimulated CheZ mutant cells is on the border of the working range of the motor, while experiments on mutant cells lacking $CheA_s$, which plays a role in localizing CheZ to the receptor cluster [12], suggest that CheZ mutant cells can chemotax. This raises an interesting question, which to our knowledge has not been studied yet: How strongly does the efficiency of chemotaxis depend upon the concentration of $CheY_p$ in the adapted state? In particular, how well must that be inside the working range of the motor? It is conceivable that cells with $[Y_p]$ at the high end of the motor's working range can chemotax, albeit less efficiently. Another possibility is that CheZ mutant cells can chemotax, because $[Y_p]$ forms spatial gradients inside CheZ mutant cells [2]: while $[Y_p]$ at some motors will be outside the motor's working range, $[Y_p]$ at other motors might be inside the working range of the motor.

But perhaps the most likely explanation is that phosphorylation of CheB by $CheA_p$ provides a negative feedback loop on the activity of the receptor cluster that tends to keep the concentration of $CheY_p$ within a certain range. The concentration of $CheY_p$ in the adapted state is determined by the activity of the receptor cluster in the adapted state, which is controlled by the activity of the methylation and demethylation enzymes CheR and CheB, respectively. $CheA_p$ cannot only phosphorylate CheY, but also CheB. Moreover, phosphorylated CheB has a higher demethylation activity than unphosphorylated CheB. Since CheY and CheB compete with one another for phosphorylation by $CheA_p$, the concentration of phosphorylated CheB increases as $[Y_p]$ increases and [Y] decreases [35]. However, since phosphorylated CheB has a higher demethylation activity, this tends to lower the activity of the receptor cluster, which in turn tends to *lower* $[Y_p]$. In our model, the activity of the receptor cluster is assumed to be the same for wild-type and CheZ mutant cells, and it was chosen such that the concentration of $CheY_p$ in adapted wild-type cells is within the working range of the motor. Yet, it is conceivable that because of the negative feedback loop, the activity of the receptor cluster in the adapted state is lower in CheZ mutant cells than in CheZ wild-type cells. This would lower the concentration of $CheY_p$ in the CheZ mutant cells and could bring it within the motor's range.

The response to other attractants

Vaknin and Berg measured not only the response to the addition to serine, but also the response of $[Y_pZ]$ to changes in aspartate concentration [2]. They found differences in the response between CheZ wild-type cells and CheZ mutant cells when α-methylaspartate was used as an attractant with $CheR^-CheB^-$ cells expressing *only* the aspartate receptor, Tar.

However, no differences were detected when these experiments were repeated with either aspartate or α-methylaspartate in wild-type cells. In our model, the overall response of $[Y_pZ]$ to changes in ligand concentration [L] is determined by two independent modules connected in series: $[Y_pZ](\beta k_0([L]))$. A different attractant only leads to a different response of the receptor cluster, $\beta_{k0}([L])$: the response of $[Y_pZ](\beta k_0)$ to changes in the activity of the receptor cluster βk_0 is assumed to be independent of the type of attractant—while $[Y_pZ](\beta k_0)$ depends upon the nature of CheZ, it is the same for serine and aspartate. Our model would therefore predict that the response to aspartate also differs between CheZ wild-type cells and CheZ mutant cells, in contradiction with the experimental results of Vaknin and Berg [2]. It is conceivable that to explain these observations, the spatial organization of the receptor cluster, in particular the spatial position of CheZ with respect to the aspartate and serine receptors, has to be taken into account, and that a full particle-based model [36,37] is required to explain the response to both aspartate and serine.

Methods

The canonical model of the intracellular chemotaxis network of *E. coli* is given by the chemical reactions shown in Equations 1–3. When CheA and CheZ are colocalized at the receptor cluster, the concentration profiles of CheY and $CheY_p$ are uniform in space, and the concentrations can be obtained by solving the following chemical rate equations:

$$\frac{\partial[Y_p]}{\partial t} = k_3[A_pY] - k_4[Z][Y_p] + k_5[Y_pZ] \quad (10)$$

$$\frac{\partial[Y]}{\partial t} = k_6[Y_pZ] - k_1[A_p][Y] + k_2[A_pY] \quad (11)$$

$$\frac{\partial[A]}{\partial t} = k_3[A_pY] - \beta k_0[A] \quad (12)$$

$$\frac{\partial[A_p]}{\partial t} = \beta k_0[A] + k_2[A_pY] - k_1[A_p][Y] \quad (13)$$

$$\frac{\partial[A_pY]}{\partial t} = k_1[A_p][Y] - (k_2+k_3)[A_pY] \quad (14)$$

$$\frac{\partial[Z]}{\partial t} = (k_5+k_6)[Y_pZ] - k_4[Z][Y_p] \quad (15)$$

$$\frac{\partial[Y_pZ]}{\partial t} = k_4[Z][Y_p] - (k_5+k_6)[Y_pZ] \quad (16)$$

Here, [X] denotes the concentration of species X.

When CheZ cannot bind the receptor cluster and thus diffuses in the cytoplasm, concentration gradients of CheY and $CheY_p$ will form. We will assume that the cell is cylindrically symmetric, and we will integrate out the lateral dimensions y and z. We thus consider a simplified 1-D model, with concentrations as a function of x. This leads to the following reaction-diffusion equations:

$$\frac{\partial[Y_p]}{\partial t} = D\frac{\partial^2[Y_p]}{\partial x^2} + k_3[A_pY]\delta(x) - k_4[Z][Y_p] + k_5[Y_pZ] \quad (17)$$

$$\frac{\partial[Y]}{\partial t} = D\frac{\partial^2[Y]}{\partial x^2} + k_6[Y_pZ] - k_1[A_p][Y]\delta(x) + k_2[A_pY]\delta(x) \quad (18)$$

$$\frac{\partial[A]}{\partial t} = k_3[A_pY] - \beta k_0[A] \quad (19)$$

$$\frac{\partial[A_p]}{\partial t} = \beta k_0[A] + k_2[A_pY] - k_1[A_p][Y](0) \quad (20)$$

$$\frac{\partial[A_pY]}{\partial t} = k_1[A_p][Y](0) - (k_2+k_3)[A_pY] \quad (21)$$

$$\frac{\partial[Z]}{\partial t} = D\frac{\partial^2[Z]}{\partial x^2} + (k_5+k_6)[Y_pZ] - k_4[Z][Y_p] \quad (22)$$

$$\frac{\partial[Y_pZ]}{\partial t} = D\frac{\partial^2[Y_pZ]}{\partial x^2} + k_4[Z][Y_p] - (k_5+k_6)[Y_pZ] \quad (23)$$

The components CheA, $CheA_p$ and $CheA_pCheY$ are localized at one end of the cell; the unit of their concentrations is the number of molecules per area. The other components diffuse in the cell. Their concentrations, which are in units of number of molecules per volume, depend upon the position x in the cell, where x measures the distance from the pole at which CheA, $CheA_p$ and $CheA_pCheY$ are localized; only in Equations 20 and 21 is the x dependence explicitly indicated to emphasize that the $CheA_p$-CheY association rate depends on the concentration of CheY at contact. Zero-flux boundary conditions are imposed at both cell ends. The steady-state input-output relations of the network described by Equations 17–23 were obtained numerically by discretizing the system on a (1-D) grid and propagating these equations in space and time until steady state was reached.

The reaction-diffusion equations for the other models described in the main text, i.e. in section *Differential affinity and catalytic activity of CheZ* and section *Cooperativity*, were derived and solved in a similar manner.

Supporting Information

Text S1 Two independent modules connected in series.
Found at: doi:10.1371/journal.pcbi.1000378.s001 (0.09 MB PDF)

Text S2 Mapping between canonical push-pull network and chemotaxis network.
Found at: doi:10.1371/journal.pcbi.1000378.s002 (0.22 MB PDF)

Text S3 Cooperativity in the phosphatase reactions.
Found at: doi:10.1371/journal.pcbi.1000378.s003 (0.29 MB PDF)

Acknowledgments

We thank Howard Berg, Dennis Bray, Victor Sourjik, Ady Vaknin, and Sorin Tănase-Nicola for useful discussions and Ady Vaknin and Tom Shimizu for a critical reading of the manuscript.

Author Contributions

Conceived and designed the experiments: PRtW. Performed the experiments: SBvA. Analyzed the data: SBvA. Wrote the paper: SBvA PRtW.

References

1. Sourjik V, Berg HC (2000) Localization of components of the chemotaxis machinery of *Escherichia coli* using fluorescent protein fusions. Mol Microbiol 37: 740–751.
2. Vaknin A, Berg HC (2004) Single-cell FRET imaging of phosphatase activity in the *Escherichia coli* chemotaxis system. Proc Natl Acad Sci U S A 101: 17072–17077.
3. Van Albada SB, Ten Wolde PR (2007) Enzyme localization can drastically affect signal amplification in signal transduction pathways. PLoS Comput Biol 3: e195. doi:10.1371/journal.pcbi.0030195.
4. Blat Y, Eisenbach M (1996) Mutants with defective phosphatase activity show no phosphorylation-dependent oligomerization of CheZ. The phosphatase of bacterial chemotaxis. J Biol Chem 271: 1232–1236.
5. Blat Y, Eisenbach M (1996) Oligomerization of the phosphatase CheZ upon interaction with the phosphorylated form of CheY. J Biol Chem 271: 1226–1231.
6. Blat Y, Gillespie B, Bren A, Dahlquist FW, Eisenbach M (1998) Regulation of phosphatase activity in bacterial chemotaxis. J Mol Biol 284: 1191–1199.
7. Silversmith RE, Levin MD, Schilling E, Bourret RB (2008) Kinetic characterization of catalysis by the chemotaxis phosphatase CheZ. Modulation of activity by the phosphorylated CheY substrate. J Biol Chem 283: 756–765.
8. Cantwell BJ, Draheim RR, Weart RB, Nguyen C, Stewart RC, et al. (2003) CheZ phosphatase localizes to chemoreceptor patches via CheA-short. J Bacteriol 185: 2354–2361.
9. Kentner D, Sourjik V (2009) Dynamic map of protein interactions in the *Escherichia coli* chemotaxis pathway. Mol Syst Biol 5: 238.
10. Wang H, Matsumura P (1996) Characterization of the CheAs/CheZ complex: a specific interaction resulting in enhanced dephosphorylating activity on CheY-phosphate. Mol Microbiol 19: 695–703.
11. Lipkow K (2006) Changing cellular location of CheZ predicted by molecular simulations. PLoS Comput Biol 2: e39. doi:10.1371/journal.pcbi.0020039.
12. Sanatinia H, Kofoid EC, Morrison TB, S PJ (1995) The smaller of two overlapping CheA gene products is not essential for chemotaxis in *Escherichia coli*. J Bacteriol 177: 2713–2720.
13. Cluzel P, Surette M, Leibler S (2000) An ultrasensitive bacterial motor revealed by monitoring signaling proteins in single cells. Science 287: 1652–1655.
14. Sourjik V, Berg HC (2002) Binding of the Escherichia coli response regulator CheY to its target measured in vivo by fluorescence resonance energy transfer. Proc Natl Acad Sci U S A 99: 12669–12674.
15. Goldbeter A, Koshland DE Jr (1981) An amplified sensitivity arising from covalent modification in biological systems. Proc Natl Acad Sci U S A 78: 6840–6844.
16. Silversmith RE (2005) High mobility of carboxyl-terminal region of bacterial chemotaxis phos-phatase CheZ is diminished upon binding divalent cation or CheY-p substrate. Biochemistry 44: 7768–7776.
17. Wolfe AJ, Stewart RC (1993) The short form of the CheA protein restores kinase activity and chemotactic ability to kinase-deficient mutants. Proc Natl Acad Sci U S A 90: 1518–1522.
18. Swanson RV, Bourret RB, Simon MI (1993) Intermolecular complementation of the kinase activity of CheA. Mol Microbiol 8: 435–441.
19. Levit M, Liu Y, Surette M, Stock J (1996) Active site interference and asymmetric activation in the chemotaxis protein histidine kinase CheA. J Biol Chem 271: 32057–32063.
20. Ellefson DD, Weber U, Wolfe AJ (1997) Genetic analysis of the catalytic domain of the chemotaxis-associated histidine kinase CheA. J Bacteriol 179: 825–830.
21. Kott L, Braswell EH, Shrout AL, Weis RM (2004) Distributed subunit interactions in CheA contribute to dimer stability: a sedimentation equilibrium study. Biochim Biophys Acta 1696: 131–140.
22. Li M, Hazelbauer GL (2004) Cellular stoichiometry of the components of the chemotaxis signaling complex. J Bacteriol 186: 3687–3694.
23. Zhao R, Collins EJ, Bourret RB, Silversmith RE (2002) Structure and catalytic mechanism of the *E. coli* chemotaxis phosphatase CheZ. Nat Struct Biol 9: 570–575.
24. LaPorte DC, Walsh K, Koshland DE Jr (1984) The branch point effect. J Biol Chem 259: 14068–14075.
25. Bray D, Levin MD, Morton-Firth CJ (1998) Receptor clustering as a cellular mechanism to control sensitivity. Nature 393: 85–88.
26. Duke TA, Bray D (1999) Heightened sensitivity of a lattice of membrane receptors. Proc Natl Acad Sci U S A 96: 10104–10108.
27. Mello BA, Tu Y (2003) Quantitative modeling of sensitivity in bacterial chemotaxis: the role of coupling among different chemoreceptor species. Proc Natl Acad Sci U S A 100: 8223–8228.
28. Shimizu TS, Aksenov SV, Bray D (2003) A spatially extended stochastic model of the bacterial chemotaxis signaling pathway. J Mol Biol 329: 291–309.
29. Rao CV, Frenklach M, Arkin AP (2004) An allosteric model for transmembrane signaling bacterial chemotaxis. J Mol Biol 343: 291–303.
30. Mello BA, Tu Y (2005) An allosteric model for heterogeneous receptor complexes: understanding bacterial chemotaxis response to multiple stimuli. Proc Natl Acad Sci U S A 102: 17354–17359.
31. Keymer JE, Endres RG, Skoge M, Yeir M, Wingreen NS (2006) Chemosensing in *E. coli*: two regimes in two-state receptors. Proc Natl Acad Sci U S A 103: 1786–1791.
32. Endres RG, Wingreen NS (2006) Precise adaptation in bacterial chemotaxis through assistance neighborhoods. Proc Natl Acad Sci U S A 103: 13040–13044.
33. Mello BA, Tu Y (2007) Effects of adaptation in maintaining high sensitivity over a wide range of backgrounds for *Escherichia coli* chemotaxis. Biophys J 92: 2329–2337.
34. Kim C, Jackson M, Lux R, Khan S (2001) Determinants of chemotactic signal amplification in *Escherichia coli*. J Mol Biol 307: 119–135.
35. Kollmann M, Loevdok L, Bartholomé K, Timmer J, Sourjik V (2005) Design principles of a bacterial signalling network. Nature 438: 504–507.
36. van Zon JS, ten Wolde PR (2005) Simulating biochemical networks at the particle level and in time and space: Green's function reaction dynamics. Phys Rev Lett 94: 128103.
37. van Zon JS, Morelli M, Tănase-Nicola, Ten Wolde PR (2006) Diffusion of transcription factors can drastically enhance the noise in gene expression. Biophys J 91: 4350–4367.
38. Elowitz MB, Surette MG, Wolf PE, Stock JB, Leibler S (1999) Protein mobility in the cytoplasm of *Escherichia coli*. J Bacteriol 181: 197–203.
39. Stewart RC, Jahreis K, Parkinson JS (2000) Rapid phosphotransfer to CheY from a CheA protein lacking the CheY-binding domain. Biochemistry 39: 13157–13165.

Text S1
Differential affinity and catalytic activity of CheZ in E. coli *chemotaxis*

S.B. van Albada and P.R. ten Wolde
(Dated: February 9, 2009)

Two independent modules connected in series

The experiments of Vaknin and Berg [1] allow us to verify whether the receptor cluster and the intracellular signaling pathway are indeed two independent modules connected in series. Vaknin and Berg performed experiments on four bacterial strains: wild type $\mathrm{CheR}^+\mathrm{CheB}^+\mathrm{CheZ}$ cells, $\mathrm{CheR}^-\mathrm{CheB}^-\mathrm{CheZ}$ cells lacking CheR and CheB, $\mathrm{CheR}^+\mathrm{CheB}^+\mathrm{CheZ}^*$ cells with mutant CheZ proteins that cannot bind the receptor cluster, and $\mathrm{CheR}^-\mathrm{CheB}^-\mathrm{CheZ}^*$ cells lacking CheR and CheB and with CheZ^* (mutated CheZ). As discussed in the main text, we assume that $\beta k_0[L]$ is the same for wild type and CheZ mutant cells, but not for wild type and *cheRcheB* cells; in contrast, $[\mathrm{Y_pZ}](\beta k_0)$ is the same for wild type and *cheRcheB* cells, but not for wild type and CheZ mutant cells. If the receptor cluster and the chemotaxis network are two independent modules connected in series, then it should be possible to describe the response curve $[\mathrm{Y_pZ}]([\mathrm{L}])$ of each of the four strains using two of the following response curves: $[\mathrm{Y_pZ}]^{Z^{\mathrm{wt}}}(\beta k_0)$ or $[\mathrm{Y_pZ}]^{Z^*}(\beta k_0)$, and $\beta k_0^{R^+B^+}([\mathrm{L}])$ or $\beta k_0^{R^-B^-}([\mathrm{L}])$. In other words, all four response curves measured in [1] should be of the composite form $[\mathrm{Y_pZ}]^{\{Z^*,Z^{wt}\}}\left(\beta k_0^{RB\pm}([\mathrm{L}])\right)$.

Figure 1 shows that the results of Vaknin and Berg [1] are consistent with the above assumptions. The figure shows $[\mathrm{Y_pZ}]$ in cells containing wild-type CheZ as a function of $[\mathrm{Y_pZ}]$ in cells containing mutant CheZ, both for *cheRcheB* cells and cells containing CheR and CheB. These figures are obtained from Figures 5A and 5C of Ref. [1], which show the effect of mutating CheZ on the renormalized FRET response, (FRET([L])/FRET([L]=0)), for *cheRcheB* cells and cells containing CheR and CheB, respectively. The FRET signal is proportional to $[\mathrm{Y_pZ}]$, which means that these figures are proportional to $[\mathrm{Y_pZ}]([\mathrm{L}])$. Since we assume that mutating CheZ has no influence on the response of the receptor cluster to ligand, $\beta k_0([\mathrm{L}])$, each ligand concentration corresponds to a unique activity of the receptor cluster, for a given type of cells (meaning either *cheRcheB* cells or cells containing the (de)methylation enzymes). Therefore, it is meaningful to plot the FRET signal of cells with wild-type CheZ as a function of the FRET signal of CheZ mutant cells at the same ligand concentration (and hence activity of the receptor cluster), both for *cheRcheB* cells (Fig.5A of Ref. [1]) and cells containing CheR and CheB (Fig.5C of Ref. [1]). If, according to our assumptions, $\beta k_0[\mathrm{L}]$ only depends upon the presence of CheR and CheB while $[\mathrm{Y_pZ}]$ only depends upon the nature of CheZ, it should be possible to scale these curves such as to make them overlap. To be more precise, in Figure 1 there are 4 different amplitudes, corresponding to $[\mathrm{Y_pZ}]([\mathrm{L}]=0)$ for wild-type cells, cells with CheR and CheB and with mutant CheZ, *cheRcheB* cells with wild-type CheZ, and *cheRcheB* cells with mutant CheZ; the two amplitudes of $\mathrm{CheR}^+\mathrm{CheB}^+$ cells, correspond, respectively, to the x- and y-coordinate of the top-right circle, while the two amplitudes of *cheRcheB* cells correspond to the top-right black square. Because no absolute FRET signal is given in Ref. [1], each of the two curves in Fig. 1, can be scaled independently in both the x- and y-direction, such as to make the curves overlap. Figure 1 is obtained by scaling the FRET signal for the wild-type ($\mathrm{CheR}^+\mathrm{CheB}^+\mathrm{CheZ}$) cells by a factor

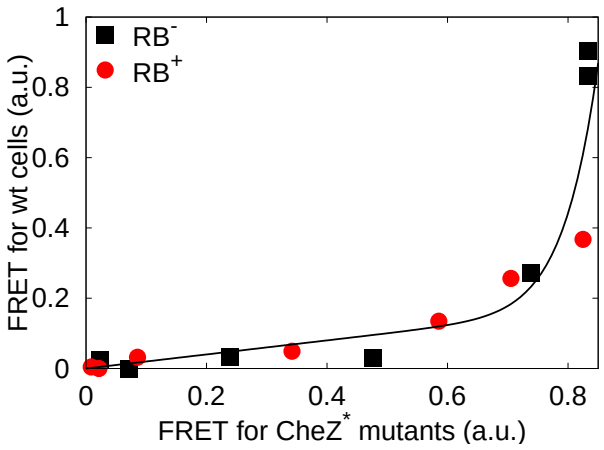

FIG. 1: The relation between the four FRET signals of Figs. 5a and 5c in [1]. FRET signals of bacterial strains that differ only in the type of phosphatase—wild-type CheZ versus a non-localizing mutant–are plotted as a function of each other. This was done both for strains lacking the adaptation proteins CheR and CheB (squares) and for strains with CheR and CheB (circles). The FRET signals on the vertical and horizontal axes are linked via equal concentrations of attractant in the reponse curves. Because of the decoupling of the response of the intracellular signal transduction pathway from the response of the receptor cluster, equal concentrations of attractant correspond to equal activities of the receptor cluster if the CheRCheB states are the same, and equal concentrations of $[\mathrm{Y_pZ}]$ correspond to equal activities of the receptor cluster if the same type of phosphatase is present. As a consequence, the two curves should overlap (see main text). This could be achieved by rescaling only the FRET signal for the wild-type bacterium by a factor 0.5.

0.5. It is seen that the curves for $CheR^+CheB^+$ cells and $CheR^-CheB^-$ cells indeed overlap. This supports the idea that the receptor cluster and the intracellular pathway are two independent modules connected in series.

Figure 1 allows us to rescale the data of Figures 5A and 5C of Ref. [1] to obtain $[Y_pZ]$ as a function of [L]. The result is shown in Figure 1A of the main text, where the maximum $[Y_pZ]$, obtained for $CheR^-CheB^-CheZ$ cells at $[L] = 0$, was set to the total CheZ concentration as reported in [2]. These response curves impose strong constraints on any model that hopes to explain the response of $CheY_pCheZ$ to the addition of serine.

[1] Vaknin A, Berg HC (2004) Single-cell FRET imaging of phosphatase activity in the *Escherichia coli* chemotaxis system. Proc Natl Acad Sci USA 101:17072–17077.

[2] Sourjik V, Berg HC (2002) Binding of the *Escherichia coli* response regulator CheY to its target measured in vivo by fluorescence resonance energy transfer. Proc Natl Acad Sci USA 99:12669 – 12674.

Text S2
Differential affinity and catalytic activity of CheZ in E. coli *chemotaxis*

S.B. van Albada and P.R. ten Wolde
(Dated: February 9, 2009)

Mapping between canonical push-pull network and chemotaxis network

The canonical model for the cytosolic signal transduction pathway in the *E. coli* chemotaxis system is given by Eqns. 1-3 of the main text. The system is very similar to the canonical push-pull network, given by the following chemical reactions:

$$\mathrm{E_a} + \mathrm{X} \underset{k_2}{\overset{k_1}{\rightleftharpoons}} \mathrm{E_aX} \overset{k_3}{\rightarrow} \mathrm{E_a} + \mathrm{X^*} \tag{1}$$

$$\mathrm{E_d} + \mathrm{X^*} \underset{k_5}{\overset{k_4}{\rightleftharpoons}} \mathrm{E_dX^*} \overset{k_6}{\rightarrow} \mathrm{E_d} + \mathrm{X} \tag{2}$$

In steady state, a direct mapping is possible between both networks. This can be seen by comparing the chemical rate equations and the total concentrations for the two systems:

Chemotaxis network	vs.	Canonical push − pull network	
$\frac{\mathrm{d[Y]}}{\mathrm{dt}} = \mathrm{k_2[A_pY]} + \mathrm{k_6[Y_pZ]} - \mathrm{k_1[A_p][Y]}$	$\Leftrightarrow$	$\frac{\mathrm{d[X]}}{\mathrm{dt}} = \mathrm{k_2[E_aX]} + \mathrm{k_6[E_dX^*]} - \mathrm{k_1[E_a][X]}$	(3)
$\frac{\mathrm{d[Y_p]}}{\mathrm{dt}} = \mathrm{k_5[Y_pZ]} + \mathrm{k_3[A_pY]} - \mathrm{k_4[Z][Y_p]}$	$\Leftrightarrow$	$\frac{\mathrm{d[X^*]}}{\mathrm{dt}} = \mathrm{k_5[E_dX^*]} + \mathrm{k_3[E_aX]} - \mathrm{k_4[E_d][X^*]}$	(4)
$\frac{\mathrm{d[Y_pZ]}}{\mathrm{dt}} = \mathrm{k_4[Z][Y_p]} - (\mathrm{k_5} + \mathrm{k_6})\mathrm{[Y_pZ]}$	$\Leftrightarrow$	$\frac{\mathrm{d[E_dX^*]}}{\mathrm{dt}} = \mathrm{k_4[E_d][X^*]} - (\mathrm{k_5} + \mathrm{k_6})\mathrm{[E_dX^*]}$	(5)
$\frac{\mathrm{d[Z]}}{\mathrm{dt}} = -\frac{\mathrm{d[Y_pZ]}}{\mathrm{dt}}$	$\Leftrightarrow$	$\frac{\mathrm{d[E_d]}}{\mathrm{dt}} = -\frac{\mathrm{d[E_dX^*]}}{\mathrm{dt}}$	(6)
$\frac{\mathrm{d[A_pY]}}{\mathrm{dt}} = \mathrm{k_1[A_p][Y]} - (\mathrm{k_2} + \mathrm{k_3})\mathrm{[A_pY]}$	$\Leftrightarrow$	$\frac{\mathrm{d[E_aX]}}{\mathrm{dt}} = \mathrm{k_1[E_a][X]} - (\mathrm{k_2} + \mathrm{k_3})\mathrm{[E_aX]}$	(7)
$\frac{\mathrm{d[A_p]}}{\mathrm{dt}} = -\frac{\mathrm{d[A_pY]}}{\mathrm{dt}} - \frac{\mathrm{d[A]}}{\mathrm{dt}}$	$\Leftrightarrow$	$\frac{\mathrm{d[E_a]}}{\mathrm{dt}} = -\frac{\mathrm{d[E_aX]}}{\mathrm{dt}}$	(8)
$\frac{\mathrm{d[A]}}{\mathrm{dt}} = \mathrm{k_3[A_pY]} - \beta\mathrm{k_0[A]}$			(9)
$\mathrm{[Y]_T} = \mathrm{[Y]} + \mathrm{[Y_p]} + \mathrm{[Y_pZ]} + \mathrm{[A_pY]}$	$\Leftrightarrow$	$\mathrm{[X]_T} = \mathrm{[X]} + \mathrm{[X^*]} + \mathrm{[E_aX]} + \mathrm{[E_dX^*]}$	(10)
$\mathrm{[Z]_T} = \mathrm{[Z]} + \mathrm{[Y_pZ]}$	$\Leftrightarrow$	$\mathrm{[E_d]_T} = \mathrm{[E_d]} + \mathrm{[E_dX^*]}$	(11)
$\mathrm{[A_p]_T} = \mathrm{[A_p]} + \mathrm{[A_pY]} = \mathrm{[A]_T} - \mathrm{[A]}$	$\Leftrightarrow$	$\mathrm{[E_a]_T} = \mathrm{[E_a]} + \mathrm{[E_aX]}$	(12)

As $\frac{\mathrm{dA}}{\mathrm{dt}}$ in Eqn. 8 equals zero in steady state, it follows that the steady state of the chemotaxis model with total concentrations $\mathrm{[Y]_T}$, $\mathrm{[Z]_T}$ and $\mathrm{[A_p]_T}$ is identical to the steady state of a push-pull network with total concentrations $\mathrm{[X]_T}$, $\mathrm{[E_d]_T}$ and $\mathrm{[E_a]_T}$, respectively. The remaining concentration of unphosphorylated A is then $\mathrm{[A]} = \mathrm{[A]_T} - \mathrm{[A_p]_T}$ (Eqn. 12) and $\beta\mathrm{k_0}$ equals $k_3\mathrm{[A_pY]}\mathrm{[A]}^{-1}$ (Eqn. 9). This mapping also holds for non-uniform networks with any spatial arrangement of the enzymes, e.g., with the activating enzyme localized at one end of the cell and the deactivating enzyme freely diffusive.

The canonical chemotaxis model is thus simply a push-pull network of which the concentration of activating enzyme $\mathrm{[E_a]_T}$ is tuned via the parameter βk_0 while the concentration of deactivating enzyme $\mathrm{[E_d]_T}$ is kept constant. The steady state of a push-pull network with given substrate and enzyme concentrations is fully determined by the ratio of the catalytic activities k_3/k_6 and the Michaelis-Menten constants $K_{M,a} \equiv (k_2+k_3)/k_1$ and $K_{M,d} \equiv (k_5 + k_6)/k_4$, as can be verified from the above

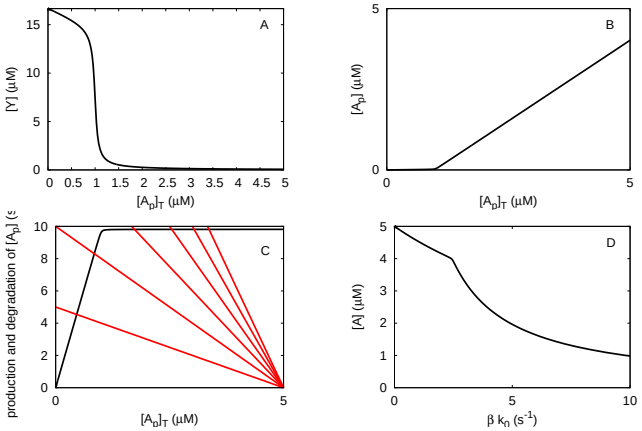

FIG. 1: Mapping of a *symmetric* network with a topology of that of the canonical *E. coli* chemotaxis network (Equations 1-3 of main text) onto a symmetric canonical push-pull network (Equations 1-2), for networks that are in the *zero-order* regime. $k_1 = k_4 = 36\ \mu\mathrm{M}^{-1}\mathrm{s}^{-1}$; $k_3 = k_6 = 10\ \mathrm{s}^{-1}$ ($K_\mathrm{M} = 0.28\ \mu$M); $S_\mathrm{T} = [\mathrm{Y}]_\mathrm{T} = 16.7\ \mu$M; $[\mathrm{E_d}]_\mathrm{T} = [\mathrm{Z}]_\mathrm{T} = 1\ \mu$M; $[\mathrm{A}]_\mathrm{T} = 5\mu$M. In panel C: the black line is given by the right-hand side of Eq. 14, i.e. $k_1[\mathrm{A_p}]([\mathrm{A_p}]_\mathrm{T})[\mathrm{Y}]([\mathrm{A_p}]_\mathrm{T})$; the red lines are given by the left-hand side of Eq. 14, i.e. $\beta k_0([\mathrm{A}]_\mathrm{T} - [\mathrm{A_p}]_\mathrm{T})$; the different red lines correspond to different values of βk_0 : $\beta k_0 = 1, 2, 3, 4, 5, 6\,\mathrm{s}^{-1}$. The intersection of the black and red curves yields $[\mathrm{A_p}]_\mathrm{T}$ as a function of βk_0. When $[\mathrm{A_p}]_\mathrm{T}$ is determined, the state of the system is fully determined.

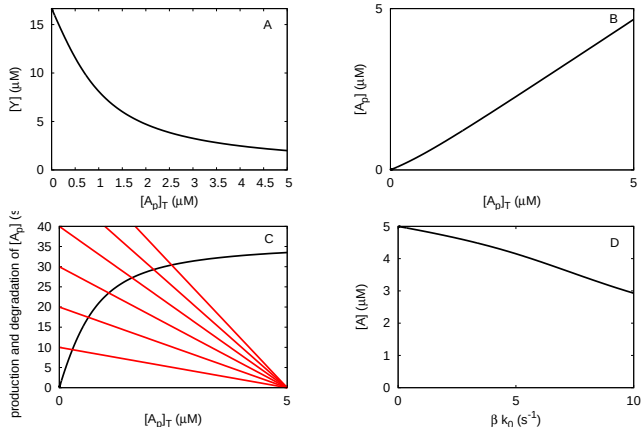

FIG. 2: Mapping of a *symmetric* network with a topology of that of the canonical *E. coli* chemotaxis network (Equations 1-3 of main text) onto a symmetric canonical push-pull network (Equations 1-2), for networks that are in the *linear* regime. The different red lines correspond to different values of βk_0 : $\beta k_0 = 2, 4, 6, 8, 10, 12\,\mathrm{s}^{-1}$. $k_1 = k_4 = 3.6\ \mu\mathrm{M}^{-1}\mathrm{s}^{-1}$; $k_3 = k_6 = 100\ \mathrm{s}^{-1}$ ($K_\mathrm{M} = 28\ \mu$M); $S_\mathrm{T} = [\mathrm{Y}]_\mathrm{T} = 16.7\ \mu$M; $[\mathrm{E_d}]_\mathrm{T} = [\mathrm{Z}]_\mathrm{T} = 1\ \mu$M; $[\mathrm{A}]_\mathrm{T} = 5\mu$M.

system of equations. Therefore, the steady state of the chemotaxis model is fully determined by the same combination of parameters, together with $\beta\mathrm{k}_0$. In particular, we can, without loss of generality, set k_2 and k_5 equal to zero—they only affect the response via their effect on the Michaelis-Menten constants.

It turns out that this mapping between a canonical push-pull network and a network with a topology of that of the chemotaxis system, is particularly useful for understanding the response of $[\mathrm{Y_p}]$ and $[\mathrm{Y_pZ}]$ and hence the FRET signal to changes in the activity of the receptor cluster βk_0. This is illustrated in Figures 1 and 2 for a spatially uniform network in the zero-order and linear regime, respectively; as discussed in [3], this also corresponds to a push-pull network in which the enzymes are colocalized at one end of the cell. In steady state, the chemotaxis network obeys the following relation:

$$\beta k_0[\mathrm{A}] = k_1[\mathrm{A_p}][\mathrm{Y}], \qquad (13)$$

where we have assumed that $k_2 = 0$. The idea is now that $[\mathrm{A_p}]$ and $[\mathrm{Y}]$ are fully determined by the total concentration of phosphorylated CheA, $[\mathrm{A_p}]_\mathrm{T} \equiv [\mathrm{A_p}] + [\mathrm{A_pY}]$, as in a canonical push-pull network: $[\mathrm{A_p}] \equiv [\mathrm{A_p}]([\mathrm{A_p}]_\mathrm{T})$ and $[\mathrm{Y}] \equiv [\mathrm{Y}]([\mathrm{A_p}]_\mathrm{T})$. The functions $[\mathrm{Y}]([\mathrm{A_p}]_\mathrm{T})$ and $[\mathrm{A_p}]([\mathrm{A_p}]_\mathrm{T})$ can be obtained analytically [4], and they are shown in Figs. 1-2A and 1-2B, respectively. The concentration of $[\mathrm{A_p}]_\mathrm{T}$, in turn, is controlled by the value of βk_0. To obtain $[\mathrm{A_p}]_\mathrm{T}$ as a function of βk_0, we rewrite the above equation as

$$\beta k_0\,([\mathrm{A}]_\mathrm{T} - [\mathrm{A_p}]_\mathrm{T}) = k_1[\mathrm{A_p}]([\mathrm{A_p}]_\mathrm{T})[\mathrm{Y}]([\mathrm{A_p}]_\mathrm{T}), \qquad (14)$$

where $[\mathrm{A}]_\mathrm{T} \equiv [\mathrm{A}] + [\mathrm{A_p}]_\mathrm{T}$ is the total concentration of CheA. This equation can now be solved for $[\mathrm{A_p}]_\mathrm{T}$ as a function of βk_0. The behavior of the solution can be understood by plotting the left-hand side and the right-hand side of the above equation separately, as is illustrated in Figures 1C and 2C for networks in the zero-order and linear regime, respectively; the intersection yields the value of $[\mathrm{A_p}]_\mathrm{T}$. The panels D in these figures show $[\mathrm{A}] = [\mathrm{A}]_\mathrm{T} - [\mathrm{A_p}]_\mathrm{T}$ as a function of βk_0. Since all the other concentrations $[\mathrm{Y}]$, $[\mathrm{Y_p}]$, $[\mathrm{A_pY}]$, and $[\mathrm{Y_pZ}]$ are determined by $[\mathrm{A_p}]_\mathrm{T}$, the state of the system is now fully specified.

The effect of phosphatase localization within the canonical chemotaxis model

In Ref. [1], dose response curves were measured for the binding of $\mathrm{Y_p}$ to Z as a function of the extracellular concentration of the ligand (L) serine, both for $\mathrm{CheR^+CheB^+}$ and $\mathrm{CheR^-CheB^-}$ cells. In what follows, we focus exclusively on $\mathrm{CheR^+CheB^+}$ cells. The concentration of the $\mathrm{Y_pZ}$ complex was measured in [1] via Fluorescence Resonance Energy Transfer (FRET). Figure 5c of Ref. [1] shows that there is a large difference between the dose response curves of wild-type cells as compared to those of CheZ mutant cells, which contain a non-localizing version of the phosphatase CheZ. In the following, we will verify whether the canonical chemotaxis model can explain the experimentally measured difference in the response of wild-type cells and CheZ mutant cells [1]. We show in the main text (Fig. 2) that

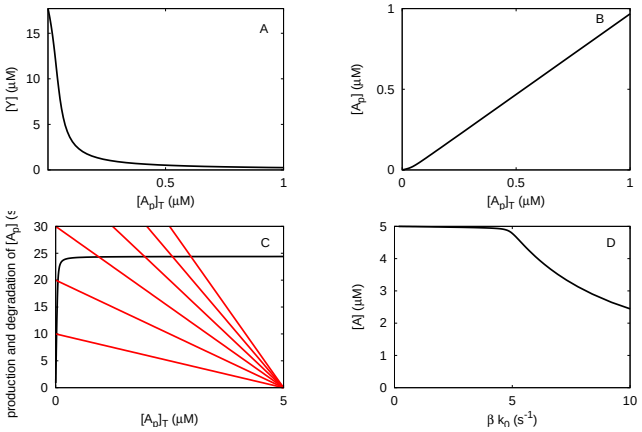

FIG. 3: Mapping of the canonical *E. coli* chemotaxis network (Equations 1-3 of main text) onto a push-pull network (Equations 1-2). The black line corresponds to the rate of $\mathrm{CheA_p}$ production as given by the right-hand side of Eq. 14, while the red lines correspond to the "decay" rate of $\mathrm{CheA_p}$ as given by the left-hand side of Eq. 14; each red line corresponds to a different value of βk_0: from left to right, $\beta k_0 = 2, 4, 6, 8, 10, 12\,\mathrm{s}^{-1}$. The intersection of the black and red lines yield $[\mathrm{A_p}]_\mathrm{T}$ in steady state. Please note that since the rate of $\mathrm{CheA_p}$ deactivation (black line) initially increases rapidly with $[\mathrm{A_p}]_\mathrm{T}$, [A] as a function of βk_0 is essentially constant and given by $[\mathrm{A}] \approx [\mathrm{A}]_\mathrm{T}$ for low values of βk_0, as shown in panel D. If $[\mathrm{A}] \approx [\mathrm{A}]_\mathrm{T}$, $[\mathrm{Y_pZ}]$ increases linearly with the activity of the receptor cluster, βk_0, since in steady state $\beta k_0[\mathrm{A}] = k_6[\mathrm{Y_pZ}]$ (see, e.g., Fig. 4). $k_1 = 100\mu\mathrm{M}^{-1}\mathrm{s}^{-1}$; $k_3 = 750\ \mathrm{s}^{-1}$; $k_4 = 5\ \mu\mathrm{M}^{-1}\mathrm{s}^{-1}$; $k_6 = 30\ \mathrm{s}^{-1}$; $[\mathrm{S}]_\mathrm{T} = [\mathrm{Y}]_\mathrm{T} = 17.9\ \mu M$; $[\mathrm{E_d}]_\mathrm{T} = [\mathrm{Z}]_\mathrm{T} = 1.1\ \mu\mathrm{M}$; $[\mathrm{A}]_\mathrm{T} = 5\mu\mathrm{M}$.

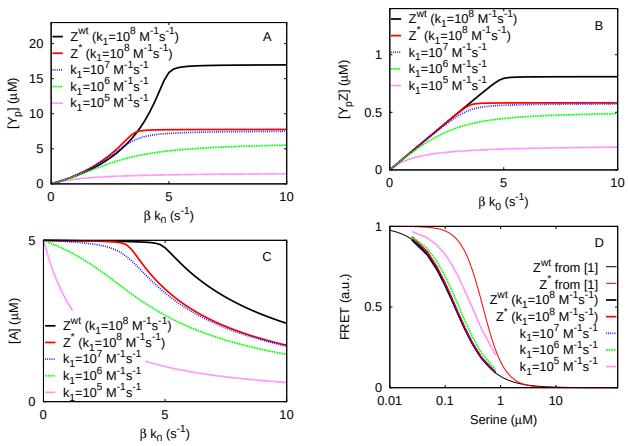

FIG. 4: Effect of varying k_1 on the response of the canonical chemotaxis model (Equations 1-3 of the main text). The thick black line corresponds to the predicted response of wild-type cells, the parameters of which are kept constant (except βk_0); the other thick lines correspond to predicted response curves of CheZ mutant cells, where each line corresponds to a different value of k_1. Shown are the response of $[\mathrm{Y_p}]$ (A), $[\mathrm{Y_pZ}]$ (B), [A] (C) to changes in the activity of the receptor cluster βk_0 and the FRET signal as a function of serine concentration (D). By construction (see text), the predicted FRET response of the wild-type cells (thick black line) coincides with the measured response [1] (thin black line). Please also note that for lower CheA-$\mathrm{CheY_p}$ association rates ($k_1 = 10^5\mathrm{M}^{-1}\mathrm{s}^{-1}$, magenta line) in CheZ mutant cells, the predicted FRET response shifts in the direction of the one measured for CheZ mutant cells (thin red line) [1]. The baseline parameters are $k_1 = 10^8\ \mathrm{M}^{-1}\mathrm{s}^{-1}$, $k_3 = 750\ \mathrm{s}^{-1}$, $k_4 = 5 \cdot 10^6\ \mathrm{M}^{-1}\mathrm{s}^{-1}$, $k_5 = 0.5\ \mathrm{s}^{-1}$, $k_6 = 30\ \mathrm{s}^{-1}$, $[\mathrm{Z}]_\mathrm{T} = 1.1\mu\mathrm{M}$, $[\mathrm{A}]_\mathrm{T} = 5\mu\mathrm{M}$ and $[\mathrm{Y}]_\mathrm{T} = 17.9\mu\mathrm{M}$ ([2]) and $D = 5\ \mu\mathrm{m}^2\mathrm{s}^{-1}$.

the canonical model cannot explain this difference in response if the only difference between wild-type cells and CheZ mutant cells is the spatial distribution of CheZ. We now address the question whether allowing also one of the other parameters (rate constants, concentrations) to be different between wild-type and CheZ mutant cells does make it possible to fit the data of Vaknin and Berg [1]. In practice, we try to fit the dose response curve of FRET vs. [serine] for both wild-type and CheZ mutant cells simultaneously, by varying the parameters for the mutant bacterium, while keeping the parameters for the wild-type bacterium fixed. The dose response curves of FRET vs. [serine] are obtained by combining the response of $[\mathrm{Y_pZ}]$ to the receptor-cluster activity βk_0 and the response of βk_0 to the concentration of added ligand, as discussed in more detail below.

Figures 4-7 show the effect of individually varying the rate constants k_1, k_3, k_4 and k_6 of the canonical model of the intracellular chemotaxis network (Equations 1-3 of the main text). For every parameter set we show the response of: A) $[\mathrm{Y_p}]$ as a function of the receptor-cluster activity βk_0; B) $[\mathrm{Y_pZ}]$ as a function of βk_0; C) [A] as a function of βk_0; D) the FRET signal as a function of added ligand (serine). Every plot shows the result for the wild-type cell with colocalized CheA and CheZ and with the baseline parameter set (black line), together with the response curves of mutant cells with diffusive CheZ, where each curve corresponds to a different value of the rate constant that is varied. The calculations were repeated for different concentrations $[\mathrm{A}]_\mathrm{T}$ and $[\mathrm{Y}]_\mathrm{T}$ with similar results (data not shown).

Figures 4C-7C show [A] as a function of βk_0. It is seen that for low values of βk_0, [A] is essentially constant, and given by $[\mathrm{A}] \approx [\mathrm{A}]_\mathrm{T}$. This is an important observation. In steady state, $\beta k_0[\mathrm{A}] = k_6[\mathrm{Y_pZ}]$ for the canonical model of the intracellular chemotaxis network. Hence, when [A] is constant, $[\mathrm{Y_pZ}]$ varies linearly with βk_0. Since the FRET signal is proportional to $[\mathrm{Y_pZ}]$, also the FRET signal varies linearly with βk_0, when [A] is constant. If the FRET signal is proportional to βk_0, then the *renormalized* FRET response is fully determined by the activity of the receptor cluster: $\mathrm{FRET}([\mathrm{L}])/\mathrm{FRET}([\mathrm{L}] = 0) = \beta k_0([\mathrm{L}])/\beta k_0([\mathrm{L}] = 0)$; it no longer depends upon parameters of the intracellular network. The observation of $[\mathrm{A}] \approx [\mathrm{A}]_\mathrm{T}$ is thus important, because a) it would justify the commonly made assumption that the renormalized FRET response reflects the activity of the receptor cluster; b) it would

mean that the canonical model cannot explain the difference in FRET response between wild-type cells and CheZ mutant cells, since the spatial distribution of CheZ is assumed to only affect the response of the intracellular network and not that of the receptor cluster.

Figure 4C shows that over the concentration range of interest (corresponding to $\beta k_0 < \beta k_0^{\rm ns} \approx 3{\rm s}^{-1}$), $[{\rm A}] \approx [{\rm A}]_{\rm T}$ is fairly constant in wild-type cells and CheZ mutant cells with the baseline parameter set. This would justify the assumption that the renormalized FRET response is a useful measure for the activity of the receptor cluster. However, by the same token, it also means that the canonical model cannot explain the experiments by Vaknin and Berg [1].

Figures 4A–7A and 4B–7B show the response of $[{\rm Y_p}]$ and $[{\rm Y_pZ}]$ as a function of βk_0. There exists a simple relation between the curves $[{\rm Y_pZ}](\beta {\rm k_0})$ and $[{\rm Y_p}](\beta {\rm k_0})$. In steady state, $[{\rm Y_p}][{\rm Z}] = {\rm K_{MZ}}[{\rm Y_pZ}]$, where $K_{\rm MZ} = (k_5 + k_6)/k_4$. Since, $[{\rm Z}] = [{\rm Z}]_{\rm T} - [{\rm Y_pZ}]$, $[{\rm Y_p}]$ can be expressed in terms of $[{\rm Y_pZ}]$ as $[{\rm Y_p}] = {\rm K_{MZ}}[{\rm Y_pZ}]/([{\rm Z}]_{\rm T} - [{\rm Y_pZ}])$. This relation immediately gives the functional form of $[{\rm Y_p}](\beta k_0)$ when $[{\rm Y_pZ}]$ depends linearly on βk_0.

We now address the question *why* [A] as a function of βk_0 is initially constant, and then suddenly decreases. To this end, we will exploit the mapping between the *E. coli* chemotaxis network and the canonical push-pull network, as illustrated in Fig. 3. In steady state, Equation 13 and Equation 14 hold. Figure 3C shows the rate of $\rm CheA_p$ production and $\rm CheA_p$ deactivation, corresponding to the left-hand side (lhs) and right-hand side (rhs) of Equation 14, respectively, as a function of $[{\rm A_p}]_{\rm T}$. The rate of $\rm CheA_p$ deactivation (rhs) is given by $k_1[{\rm A_p}]([{\rm A_p}]_{\rm T})[{\rm Y}]([{\rm A_p}]_{\rm T})$. As shown in Fig. 3B, for the *E. coli* network $[{\rm A_p}] \approx [{\rm A_p}]_{\rm T}$. Hence, the slope of the rhs is given by $k_1[{\rm Y}]([{\rm A_p}]_{\rm T})$. Fig. 3A shows the concentration of CheY as a function of the total $\rm CheA_p$ concentration, i.e. $[{\rm Y}]([{\rm A_p}]_{\rm T})$. It is seen that [Y] is high for low values of $[{\rm A_p}]_{\rm T}$; this explains the large initial slope of $k_1[{\rm A_p}][{\rm Y}]$ as a function of $[{\rm A_p}]_{\rm T}$ in Fig. 3C. Figure 3A also shows that as $[{\rm A_p}]_{\rm T}$ is increased, [Y] decreases strongly. This explains the strong drop in the slope of $k_1[{\rm A_p}][{\rm Y}]$ (rhs) as $[{\rm A_p}]_{\rm T}$ is increased. Because $k_1[{\rm A_p}][{\rm Y}]$ (rhs Eq. 14) initially rises rapidly with $[{\rm A_p}]_{\rm T}$ and then levels off abruptly, the intersection with the curve $\beta k_0[{\rm A}]$ (lhs Eq. 13), which determines the steady state, initially occurs for very low values of $[{\rm A_p}]_{\rm T}$ as βk_0 is increased from zero. Only when the activity of the receptor cluster, βk_0, is such that the total $\rm CheA_p$ concentration becomes large enough to decrease [Y], does $[{\rm A_p}]$ increase and [A] decrease, as shown in Fig. 3D. Put differently, initially the $\rm CheA_p$ molecules that are produced, immediately react with CheY molecules to yield CheA molecules again. This keeps the concentration of $\rm CheA_p$ low. However, in this process, the concentration of CheY does decrease, and this reduces the rate at which $\rm CheA_p$ molecules are dephosphorylated. At some point, [Y], and hence the rate of $\rm CheA_p$ dephosphorylation, has decreased so much, that the concentration of $\rm CheA_p$ will rapidly rise.

Figs. 1 and 2 show the results for a symmetric push-pull network in the zero-order and first-order regime, respectively. For the zero-order network, it is seen that $[{\rm A}](\beta k_0)$ has two distinct regimes. The first corresponds to the regime in which the phosphatase activity is larger than the kinase activity, and [Y] is large (Fig. 1A); note that since the network is zero-order, also the concentration of [A] is low (Fig. 1B). Because [Y] is high in this regime, the initial slope of $k_1[{\rm A_p}][{\rm Y}]$ as a function of $[{\rm A_p}]_{\rm T}$ is large (Fig. 1C). The second regime corresponds to the one in which the kinase activity exceeds the phosphatase activity; $[{\rm Y_p}]$ is large and [Y] is low; because [Y] is now very low, the slope is essentially reduced to zero (Fig. 1C). The situation differs markedly for a push-pull network in the linear regime. In this regime, the concentration of [Y] changes gradually as a function of $[{\rm A_p}]_{\rm T}$ (Fig. 2A) and this leads to a gradual change in the slope of $k_1[{\rm A_p}][{\rm Y}]$ as a function of $[{\rm A_p}]_{\rm T}$ (Fig. 2C). This gradual change in the slope manifests itself as a gradual change in $[{\rm A}](\beta k_0)$ (Fig. 2D).

We are now in a position to understand how the response curves change as the rate constants are varied. As k_1 is decreased, the push-pull network becomes more linear, as a result of which the concentration of $[{\rm Y_p}]$ decreases more gradually as $[{\rm A_p}]_{\rm T}$ increases. Moreover, as k_1 is decreased, the rate at which $\rm CheA_p$ molecules are dephosphorylated decreases. These two effects combine to yield a more gradual change in the rate of $\rm CheA_p$ deactivation (the rhs of Eq. 14) as a function of $[{\rm A_p}]_{\rm T}$; as seen for the symmetric push-pull network in the linear regime (Fig. 2C), such a gradual change in $k_1[{\rm A_p}][{\rm Y}]$ as a function of $[{\rm A_p}]_{\rm T}$, means that [A] starts to decrease at lower values of βk_0 and then does so more gradually (see Fig. 4). When k_3 is decreased, the network enters the zero-order regime more deeply, and the response becomes similar to that of the symmetric push-pull network in the zero-order regime (compare Figs. 1 and 5). When k_4 is decreased, [Y] decreases at lower values of $[{\rm A_p}]_{\rm T}$ and does so more gradually, since the network becomes more linear; consequently, [A] starts to decrease at lower values of βk_0 (Fig. 6C). Lastly, when k_6 is decreased, [Y] decreases more sharply for lower values of $[{\rm A_p}]_{\rm T}$. As a result, $[{\rm A}](\beta k_0)$ starts to decrease at lower values of βk_0 and then does so more strongly (Fig. 7C). Please note that in all cases, when [A] is no longer constant and equal to $[{\rm A}]_{\rm T}$, $[{\rm Y_pZ}](\beta k_0)$ is no longer a straight line, but becomes a concave function (Figs. 4B–7B). As discussed in the main text, such a concave function for CheZ mutant cells over the concentration range of interest, could make it possible to simultaneously fit the measured dose-response curves for wild-type and CheZ mutant cells [1].

To show the degree of agreement with experiment that can be obtained, we present in Figures 4D–7D the predictions of the canonical model for the FRET signal as a function of ligand concentration for both wild-type and CheZ mutant cells. These curves are obtained as follows. First, we note that $[{\rm Y_pZ}]([{\rm L}])$ is given by $[{\rm Y_pZ}](\beta k_0([{\rm L}]))$. For wild-type cells, $[{\rm Y_pZ}]$ is linear in βk_0, which means

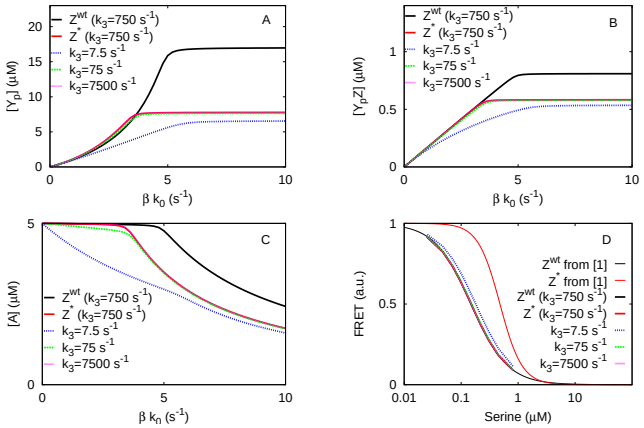

FIG. 5: Effect of k_3 on the response of the canonical chemotaxis model (Equations 1-3 of the main text). Shown are the response of $[Y_p]$ (A), $[Y_pZ]$ (B), $[A]$ (C) to changes in the activity of the receptor cluster βk_0 and the FRET signal as a function of serine concentration (D). The baseline parameters are given in Fig. 4.

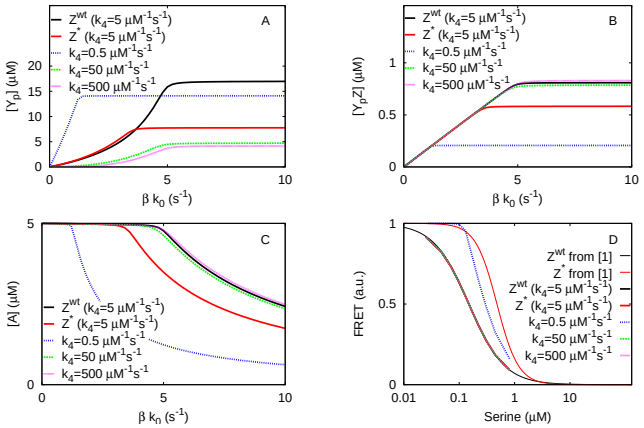

FIG. 6: Effect of k_4 on the response of the canonical chemotaxis model (Equations 1-3 of the main text). Shown are $[Y_p]$ (A), $[Y_pZ]$ (B), $[A]$ (C) as a function of βk_0, and the FRET signal as a function of serine concentration (D). Please note that for a lower CheZ-CheY$_p$ association rate ($k_4 = 10^5$ M^{-1}s^{-1}, blue line) in CheZ mutant cells, the predicted FRET response of CheZ mutant cells agrees fairly well with the experimentally measured one (thin red line) [1]. The baseline parameters are given in Fig. 4.

that apart from a proportionality factor, $\beta k_0([L])$ is given by $[Y_pZ]([L])$. The latter is obtained up to a scaling factor by the FRET data in Fig. 5c of [1], which can be fitted to a Hill function. Hence, $\beta k_0([L])$ can be described by a Hill function $\beta k_0([L]) = \frac{C_1}{1+([L]/K_D)^{n_H}}$, where K_D and n_H can directly be obtained from the fit to the FRET data. The constant C_1 is given by the value of βk_0 at zero ligand concentration, i.e. in the non-stimulated state: $C_1 = \beta k_0^{ns}$; we chose the constant such that $[Y_p](\beta k_0^{ns}) \approx 3\mu$M, which is in the middle of the working range of the motor. Note that, by construction, the FRET response of wild-type cells, as predicted by the canonical model, agrees with that observed experimentally. The FRET curves for the CheZ mutant cells can now be obtained by combining the computed $[Y_pZ](\beta k_0)$ for these cells with $\beta k_0([L])$, which is assumed to be the same for both wild-type cells and CheZ mutant cells; thus, not only K_D and n_H are the same, but also βk_0^{ns} and hence C_1; as discussed in the main text, this relies on the assumption that there is no feedback from CheY to the activity of the receptor cluster, which could affect the value of βk_0 in the non-stimulated state.

The results of this procedure are shown in Figs. 4D-7D. For the wild-type cell, the predicted dose-response curve indeed coincides with the experimental curve as measured in [1], while for the mutant cells the predicted response curves typically deviate from those measured experimentally. A good simultaneous fit to the dose-response curves of the wild-type and CheZ mutant cells can be obtained by assuming a lower value of the catalyic rate k_6 for the CheZ mutant cells (see Fig. 7D). Both the lower sensitivity for the mutant cells as well as the increased sharpness of the dose resonse curve are reproduced if the catalytic activity of CheZ, k_6, is approximately ten times lower for the mutant cells than for the wild-type cells.

Although the fit to the dose response curves is good, it can also be seen from Figs. 7A and 7B that the concentration of CheY$_p$ and the concentration of CheY$_p$CheZ are at their maximum values for the mutant cells when they are in their non-stimulated state, i.e. when $\beta k_0 \approx \beta k_0^{ns}$. If the level of $[Y_p]$ is at its maximum level, it is impossible for the mutant cells to respond to repellents. Furthermore, since $[Y_p]$ is constant as a function of βk_0 around the non-stimulated state, βk_0 must be lowered

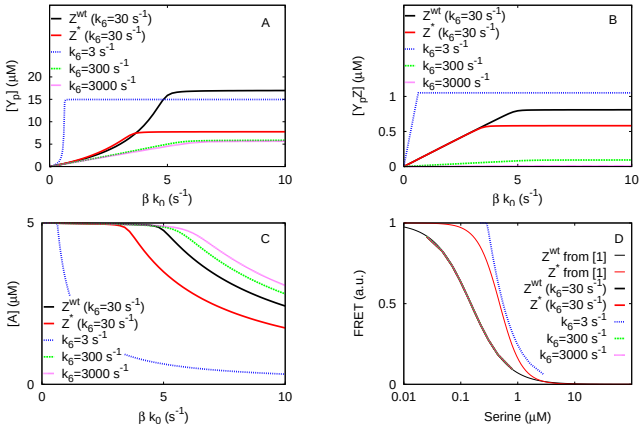

FIG. 7: Effect of changing k_6 on the response of the canonical chemotaxis model (Equations 1-3 of main text). Shown are: $[Y_p](\beta k_0)$ (A), $[Y_pZ](\beta k_0)$ (B), $[A](\beta k_0)$ (C), FRET([serine]) (D). Please note that for a lower phosphatase activity in CheZ mutant cells ($k_6 = 3$ s^{-1}, blue line), the predicted FRET response agrees quite well with that measured experimentally (thin red line) [1]. The baseline parameters are given in Fig. 4.

by a large amount upon the addition of attractant before the mutant cells can respond. Chemotaxis thus seems impossible for the mutant cells. However, it is known that bacteria with a non-localizing phosphatase are able to chemotax towards attractants, although less efficiently than wild-type bacteria [6]. Hence, while a lower catalytic activity of diffusive CheZ with respect to localized CheZ can explain the experimentally observed change in the dose-response curve [1], it seems inconsistent with the observation that the mutants are still able to chemotax.

A similar behaviour is seen in Fig. 6 for a ten times lower value of the association rate k_4 of $CheY_p$ to CheZ: although the dose response curves for wild-type and mutant bacteria can be simultaneously fitted, the mutant cells would adapt to the maximum values of both $CheY_p$ and $CheY_pCheZ$. Furthermore, $[Y_pZ]$ is much lower for the mutant cell than for the wild-type cell as can be seen from Fig. 6B, in contrast with the observations in [1]. We therefore argue that the canonical model of the intracellular chemotaxis network needs to be refined.

[1] Vaknin A, Berg HC (2004) Single-cell FRET imaging of phosphatase activity in the *Escherichia coli* chemotaxis system. Proc Natl Acad Sci USA 101:17072–17077.

[2] Sourjik V, Berg HC (2002) Binding of the *Escherichia coli* response regulator CheY to its target measured in vivo by fluorescence resonance energy transfer. Proc Natl Acad Sci USA 99:12669 – 12674.

[3] Van Albada SB, Ten Wolde PR (2007) Enzyme localization can drastically affect signal amplfication in signal transduction pathways. PLoS Comp Biol 3:e195.

[4] Goldbeter A, Koshland, Jr DE (1981) An amplified sensitivity arising from covalent modification in biological systems. Proc Natl Acad Sci USA 78:6840–6844.

[5] Wang H, Matsumura P (1996) Characterization of the $CheA_s$/CheZ complex: a specific interaction resulting in enhanced dephosphorylating activity on CheY-phosphate. Mol Microbiol 19:695–703.

[6] Sanatinia H, Kofoid EC, Morrison TB, S PJ (1995) The smaller of two overlapping CheA gene products is not essential for chemotaxis in *Escherichia coli*. J Bacteriol 177:2713–2720.

Text S3
Differential affinity and catalytic activity of CheZ in E. coli *chemotaxis*

S.B. van Albada and P.R. ten Wolde
(Dated: February 9, 2009)

Cooperativity in the phosphatase reactions

Cooperativity in the dephosphorylation of $CheY_p$ by CheZ was first shown by Blat et al. [1]. A quantitative study of the cooperativity in $CheY_p$ dephosphorylation was presented in [2]. In this section we discuss a model of CheZ activity that can describe the experimental data of Blat et al. [2]. We will show that this model can accurately reproduce the experimental data of Eisenbach *et al.*, although, as we will discuss, it seems likely that some of the rate constants obtained might differ from those *in vivo*. We also note here for clarity that since the experiments were performed *in vitro* and no $CheA_s$ was present, the results apply to dephosphorylation of $CheY_p$ by diffusive CheZ and not to CheZ localized at the receptor cluster.

The model for the phosphatase activity is given by Eqs. 1 and 3 of the main text. Together with the phosphorylation reaction of CheY, this yields the following model for the experimental setup of Ref. [2]:

$$Y \overset{AcP}{\rightarrow} Y_p \tag{1}$$

$$Y_p + Z \underset{k_5}{\overset{k_4}{\rightleftharpoons}} Y_pZ \overset{k_6}{\rightarrow} Y + Z \tag{2}$$

$$Y_pZ + Y_p \underset{k_8}{\overset{k_7}{\rightleftharpoons}} (Y_p)_2Z \overset{k_9}{\rightarrow} Y + Y_pZ \tag{3}$$

Here, the first reaction describes the phosphorylation reaction in the *in vitro* experimental setup of Eisenbach *et al.* [2], in which CheY is continuously phosphorylated by acetyl phosphate AcP. Please note that Z corresponds to one CheZ *dimer*.

Figure 1c in [2] shows the results on the kinetics of CheY dephosphorylation by CheZ. $CheY_p$, in the presence of acetyl phosphate, was instantaneously mixed with a small amount of CheZ. The total concentration $[CheY]_T$ was 5 μM and the concentration of CheZ dimers was 0.1 μM–much lower than in a living cell. The rate of phosphorylation of CheY by AcP was also low, 0.207 s^{-1} [2]. Four relevant quantities can be extracted from the phosphorylation kinetics in Fig. 1c of [2], i) the time duration of the delay, ii) the value of $d[Y_p]/dt$ after the transient, iii) the size (and presence) of the undershoot before the steady state is reached and iv) the steady state concentration of $CheY_p$.

Figure 1 shows the effect of individually varying the parameters on the phosphatase kinetics. We assume that the two backward rates k_5 and k_8 are zero, since the dissocation rates are smaller than the catalytic rates [3]. The initial delay is determined by the time it takes for $[(Y_p)_2Z]$ to reach its maximum level. In the limit that

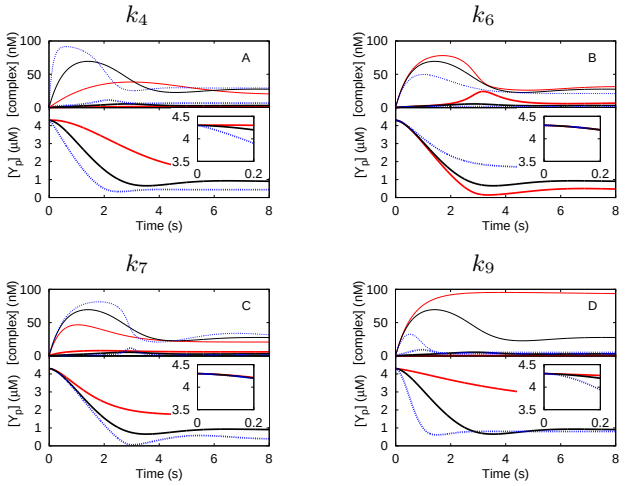

FIG. 1: Effect of varying the parameters of the cooperative model (Equations 2–3) on the phosphatase kinetics. The upper panels show the concentrations of $[(Y_p)_2Z]$ (upper three curves) and of $[Y_pZ]$ (lower three curves) as functions of time. The lower panels show the evolution of the concentration of $CheY_p$ upon addition of CheZ. The concentration of $CheY_p$ does not go to zero because CheY is continuously phosphorylated by AcP, as in the experimental setup [2]. The insets show a magnification of the initial delay. A. Effect of k_4. B. Effect of k_6. C. Effect of k_7. D. Effect of k_9. The parameter values are 0.2 (red), 1 (black) and 5 (blue) times the baseline parameters of Fig. 3.

the binding of $CheY_p$ to $CheY_pCheZ$ is much faster than the association of $CheY_p$ to CheZ, i.e. if $k_7 \gg k_4$, the delay is dominated by k_4 (see Fig. 1A). The association rate k_4 is, however, sufficiently fast, such that after this transient, a steady state can be reached in which CheZ is predominantly in the state $(Y_p)_2Z$. In this regime, the overall phosphatase activity per CheZ dimer is to a good approximation given by k_9, and the slope of $[Y_p](t)$ is given by $k_9[Z]_T$.

The undershoot of $[Y_p](t)$ in Fig. 1 arises from the subtle interplay between a number of factors. After a short transient of about 0.1 s, essentially all CheZ dimers are in the $(Y_p)_2Z$ state. In this state, the phosphatase activity of the CheZ dimers is high, and the concentration of $CheY_p$ drops rapidly. Importantly, when a $CheY_p$ molecule in a $(Y_p)_2Z$ complex is dephosphorylated, a Y_pZ complex is produced. When the concentration of $CheY_p$ is high, this complex can immediately rebind another $CheY_p$ molecule, from which another catalysis reaction can take place. However, after about $1-2$ s, the concentration of $CheY_p$ has dropped so much that the rate

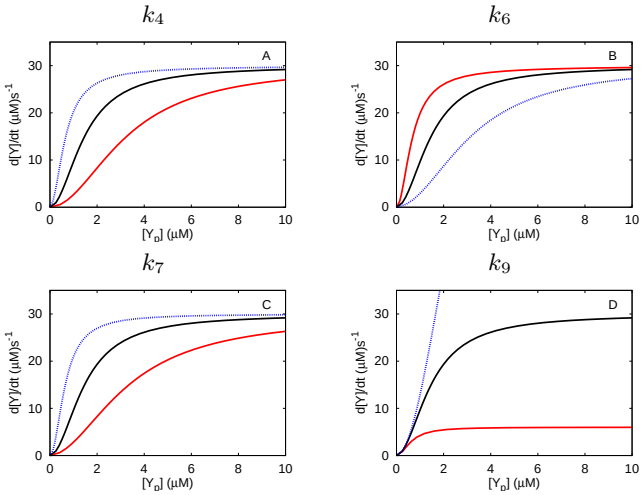

FIG. 2: Effect of varying the parameters of the cooperative model (Equations 2–3) on the specific phosphatase activity. A. Effect of k_4. B. Effect of k_6. C. Effect of k_7. D. Effect of k_9. The parameter values were 0.2 (red), 1 (black) and 5 (blue) times the baseline parameters of Fig. 3.

of association between $\mathrm{CheY_p}$ and $\mathrm{CheY_pCheZ}$ decreases significantly. The concentration of $(\mathrm{Y_p})_2\mathrm{Z}$ now decreases, while the concentration of $\mathrm{Y_pZ}$ *increases*. Since the phosphatase activity of $\mathrm{Y_pZ}$ is lower than that of $(\mathrm{Y_p})_2\mathrm{Z}$, the concentration of $\mathrm{CheY_p}$ will now increase again, until a new steady state is finally reached.

One would expect that the steady state concentration of $\mathrm{CheY_p}$ can only decrease if any of the four association constants or catalytic activities is raised. Interestingly, this does not hold for k_6 (see Fig. 1B). While the total steady state catalytic activity of $\mathrm{Y_pZ}$, as given by $k_6[\mathrm{Y_pZ}]$, increases for larger values of k_6, the total catalytic activity of $(\mathrm{Y_p})_2\mathrm{Z}$, $k_9[(\mathrm{Y_p})_2\mathrm{Z}]$, decreases by a larger amount; the reason is that as k_6 increases, the concentration of $(\mathrm{Y_p})_2\mathrm{Z}$ decreases. Consequently, the total steady state catalytic activity of $\mathrm{Y_pZ}$ and $(\mathrm{Y_p})_2\mathrm{Z}$ together decreases as k_6 is raised. This increases the concentration of $\mathrm{CheY_p}$.

Figure 2a in [2] shows the specific phosphatase activity of CheZ as a function of the concentration of $\mathrm{CheY_p}$. The relevant quantities in Fig. 2a in [2] are the degree of cooperativity and the limiting value of the specific phosphatase activity. The effect of individually varying the parameters k_4, k_6, k_7 and k_9 on the specific phosphatase activity can be seen in Fig. 2. To analyse the dependence on these variables, we will first derive an expression for the phosphatase activity in steady state in the cooperative model given by Eqs. 2 and 3. First, $d[\mathrm{Z}]/dt = 0$ gives $[\mathrm{Y_p}][\mathrm{Z}] = (k_5 + k_6)/k_4[\mathrm{Y_pZ}] \equiv K_{M,1}[\mathrm{Y_pZ}]$. Next, $d[(\mathrm{Y_p})_2\mathrm{Z}]/dt = 0$ leads to $[\mathrm{Y_p}][\mathrm{Y_pZ}] = (k_8+k_9)/k_7\ [(\mathrm{Y_p})_2\mathrm{Z}] \equiv K_{M,2}[(\mathrm{Y_p})_2\mathrm{Z}]$. The total concentration of CheZ equals $[\mathrm{Z}]_\mathrm{T} = [\mathrm{Z}] + [\mathrm{Y_pZ}] + [(\mathrm{Y_p})_2\mathrm{Z}]$. Via elimination of $[(\mathrm{Y_p})_2\mathrm{Z}]$ and $[\mathrm{Z}]$, $[\mathrm{Y_pZ}]$ can be expressed

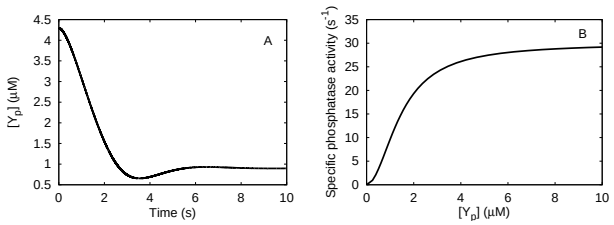

FIG. 3: Best fit of the cooperative model to Figs. 1c and 2a of [2]. The parameter values are: $k_4 = 0.36(2.0) \cdot 10^6\ \mathrm{M^{-1}s^{-1}}$, $k_6 = 7.5(5.0)\ \mathrm{s^{-1}}$, $k_7 = 3(3) \cdot 10^8\ \mathrm{M^{-1}s^{-1}}$, $k_9 = 30(10)\ \mathrm{s^{-1}}$.

as

$$[\mathrm{Y_pZ}] = \frac{[\mathrm{Z}]_\mathrm{T}[\mathrm{Y_p}]}{K_{M,1} + [\mathrm{Y_p}] + [\mathrm{Y_p}]^2/K_{M,2}}. \tag{4}$$

The concentration of the doubly-bound state is given by

$$[(\mathrm{Y_p})_2\mathrm{Z}] = [\mathrm{Y_pZ}][\mathrm{Y_p}]/K_{M,2}, \tag{5}$$

Since the production rate of CheY is equal to $k_3[\mathrm{Y_pZ}] + k_6[(\mathrm{Y_p})_2\mathrm{Z}]$, it follows that

$$\frac{d[\mathrm{Y}]}{dt} = \frac{[\mathrm{Z}]_\mathrm{T}[\mathrm{Y_p}](k_6 + k_9[\mathrm{Y_p}]/K_{M,2})}{K_{M,1} + [\mathrm{Y_p}] + [\mathrm{Y_p}]^2/K_{M,2}}. \tag{6}$$

The network behaves cooperatively if the numerator is quadratic in $[\mathrm{Y_p}]$ and the denominator only marginally depends on $[\mathrm{Y_p}]$ when $[\mathrm{Y_p}]$ is small. This is achieved if k_9 is much larger than k_6 and if $K_{M,1}$ is larger than $K_{M,2}$: in the limit that $k_6 \ll k_9$ and $K_{M,1} \gg K_{M,2}$, the dephosphorylation rate is given by

$$\frac{d[\mathrm{Y}]}{dt} = \frac{k_9[\mathrm{Z}]_\mathrm{T}[\mathrm{Y_p}]^2}{K_{M,1}K_{M,2} + [\mathrm{Y_p}]^2}. \tag{7}$$

This is a Hill function with a Hill coefficient of 2 and a concentration at which the rate is half maximal (the inflection point) given by $K_\mathrm{M}^\mathrm{eff} = \sqrt{K_{M,1}K_{M,2}}$. This can be verified from Fig. 2. An increase in either the association constant k_4 or k_7 by a factor C, or a decrease by the same factor of either the catalytic activity k_6 or k_9 leads to an increase in one of the Michaelis-Menten constants by the same factor and therefore to an increase by a factor $\sqrt{C}$ of $K_\mathrm{M}^\mathrm{eff}$. A change in k_9 by a factor C additionally leads to a C times higher limiting phosphatase activity. The value of k_9 can therefore be determined from the maximum phosphatase activity in Figure 2a in [2].

The best simultaneous fit to Figs. 1c and 2a of [2] is shown in Fig. 3. The used rate constants are $k_4 = 0.36(2.0) \cdot 10^6\ \mathrm{M^{-1}s^{-1}}$, $k_6 = 7.5(5.0)\ \mathrm{s^{-1}}$, $k_7 = 3(3) \cdot 10^8\ \mathrm{M^{-1}s^{-1}}$ and $k_9 = 30(10)\ \mathrm{s^{-1}}$. These values were also used as the baseline parameters in Fig. 2. While the best fits of the cooperative model show good agreement with the experimental data, it should be stressed that these experiments were performed *in vitro* rather than in a living bacterium. Therefore, it is

well possible that the actual rate parameters in a living cell differ from those determined here. For example, it is well known that the diffusion coefficient *in vitro* can be ten times higher than that in a living cell. This means that especially diffusion-limited association reactions can slow down *in vivo*. We assume that the value of k_7 is ten times lower *in vivo* than *in vitro*: *in vivo*, $k_7^{\rm cell} = 3 \cdot 10^7\ {\rm M}^{-1}{\rm s}^{-1}$; we assume that k_4 is unchanged, since that rate is not diffusion limited.

The full differential affinity and catalytic activity model for the intracellular chemotaxis pathway

The full model for the intracellular chemotaxis network of *E. coli* is given by the following chemical reactions (see the main text):

$$\mathrm{A} \overset{\beta k_0}{\rightarrow} \mathrm{A_p} \tag{8}$$

$$\mathrm{A_p} + \mathrm{Y} \underset{k_2}{\overset{k_1}{\rightleftharpoons}} \mathrm{A_pY} \overset{k_3}{\rightarrow} \mathrm{A} + \mathrm{Y_p} \tag{9}$$

$$\mathrm{Y_p} + \mathrm{Z} \underset{k_5}{\overset{k_4}{\rightleftharpoons}} \mathrm{Y_pZ} \overset{k_6}{\rightarrow} \mathrm{Y} + \mathrm{Z} \tag{10}$$

$$\mathrm{Y_p} + \mathrm{Z_b} \underset{k_{11}}{\overset{k_{10}}{\rightleftharpoons}} \mathrm{Y_pZ_b} \overset{k_{12}}{\rightarrow} \mathrm{Y} + \mathrm{Z_b} \tag{11}$$

$$\mathrm{Y_pZ} + \mathrm{Y_p} \underset{k_8}{\overset{k_7}{\rightleftharpoons}} (\mathrm{Y_p})_2\mathrm{Z} \overset{k_9}{\rightarrow} \mathrm{Y} + \mathrm{Y_pZ} \tag{12}$$

$$\mathrm{Y_pZ_b} + \mathrm{Y_p} \underset{k_{14}}{\overset{k_{13}}{\rightleftharpoons}} (\mathrm{Y_p})_2\mathrm{Z_b} \overset{k_{15}}{\rightarrow} \mathrm{Y} + \mathrm{Y_pZ_b} \tag{13}$$

In this model, in wild-type cells CheZ is present both bound to the receptor cluster, indicated by $\mathrm{Z_b}$, and freely diffusive. The majority of CheZ is assumed to be diffusive, but the affinity for $\mathrm{CheY_p}$ as well as the catalytic activity is much larger for the localized fraction of CheZ (for parameter values, see the caption of Fig. 4).

Fig. 4 shows the response of the concentration of $\mathrm{CheY_p}$ and the FRET signal to changes in the activity of the receptor cluster, βk_0. We assume that the FRET signal is given by: $\mathrm{FRET} \propto [\mathrm{Y_pZ}] + 2[(\mathrm{Y_p})_2\mathrm{Z}] + [\mathrm{Y_pZ_b}] + 2[(\mathrm{Y_p})_2\mathrm{Z_b}]$. It is seen that the functions $\mathrm{FRET}(\beta k_0)$ and $[\mathrm{Y_p}](\beta k_0)$ consist of two parts. In the first regime, corresponding to low concentrations of $\mathrm{CheY_p}$, the fraction of CheZ that is localized to the receptor cluster is not yet saturated. In this regime, $\mathrm{CheY_p}$ that is produced by $\mathrm{CheA_p}$ at the cluster will rapidly bind to CheZ at the cluster. While the FRET signal increases in this regime due to binding of $\mathrm{CheY_p}$ to $\mathrm{CheZ_b}$, the concentration of $\mathrm{CheY_p}$ hardly increases due to the large phosphatase activity of $\mathrm{CheZ_b}$. The second part of the response curves corresponds to the regime in which $\mathrm{CheZ_b}$ is fully saturated. In this regime, a $\mathrm{CheY_p}$ molecule that is produced at the receptor cluster, can no longer bind a CheZ dimer that is bound to the receptor cluster; it will therefore diffuse into the cytoplasm, where it will bind a diffusive CheZ dimer. This CheZ has a lower phosphatase activity than $\mathrm{CheZ_b}$ and, as a result, the concentration of $\mathrm{CheY_p}$, as well as the FRET signal, will rise rapidly.

As discussed in the main text, if the activity $\beta k_0^{\rm ns}$ of the receptor cluster is the same for wild-type and CheZ mutant cells, it is difficult to have $[\mathrm{Y_p}]^{\rm ns}$ in the working range of the motor for both types of cells. As we discuss now, a cooperative (super-linear) dependence of the phosphatase activity on $[\mathrm{Y_p}]$ makes it easier to satisfy this constraint. First, we note that the constraint that $[\mathrm{Y_p}]$ should be within the working range of the motor for both wild-type and CheZ mutant cells is satisfied more easily if $[\mathrm{Y_p}]$ for diffusive CheZ is a concave (hyperbolic) function of βk_0. Such a concave functional form can be obtained when the phosphatase activity depends super-linearly on $[\mathrm{Y_p}]$: In steady state, the kinase activity $d[\mathrm{Y_p}]/dt$ is given by $\beta k_0[\mathrm{A}] = k_1[\mathrm{A_p}][\mathrm{Y}]$ and equal to the phosphatase activity $d[\mathrm{Y}]/dt$. If $[\mathrm{A}] \approx [\mathrm{A}]_{\rm T}$, the kinase activity is proportional to βk_0, which means that in steady state the specific phosphatase activity $d[\mathrm{Y}]/dt$ is proportional to βk_0. If the specific phosphatase acitivity (and hence βk_0) increases super-linearly (up to quadratically) with $[\mathrm{Y_p}]$ for low $[\mathrm{Y_p}]$ as in the cooperative CheZ model, $[\mathrm{Y_p}]$ as a function of βk_0 has a concave form, as can also be seen in Fig. 2.

We now briefly discuss the effect of varying the rate constants and the diffusion constant on the response curves $[\mathrm{Y_p}](\beta k_0)$ and $\mathrm{FRET}(\beta k_0)$, as shown in Fig. 4. The effect of changing the parameters related to the kinase reactions, k_1 and k_3, is similar to that of changing these rate constants in the canonical model, as discussed above. In particular, as long as $[\mathrm{A}] \approx [\mathrm{A}]_{\rm T}$, the total phosphorylation rate is independent of k_1 and k_3, and $[\mathrm{Y_p}]$ and FRET are fairly insensitive to changes in these rate constants.

The parameters k_4, k_6, k_7 and k_9 correspond to dephosphorylation reactions by CheZ in the cytoplasm. Clearly, changing these rate constants only affects the second regime of the response curves $[\mathrm{Y_p}](\beta k_0)$ and $\mathrm{FRET}(\beta k_0)$, in which CheZ bound to the cluster is saturated (see Fig. 4). The influence of varying these parameters on $[\mathrm{Y_p}](\beta k_0)$ can be deduced from the corresonding panels in Fig. 2, which shows the phosphatase activity for diffusive CheZ. Since the kinase activity $\beta k_0[\mathrm{A}]$ equals in steady state the phosphatase activity $d[\mathrm{Y}]/dt$, $[\mathrm{Y_p}](\beta k_0)$ is also given by $[\mathrm{Y_p}](d[\mathrm{Y}]/dt[\mathrm{A}]_{\rm T})$. Thus, by inverting the axes of Fig. 2, one can deduce the change in $[\mathrm{Y_p}](\beta k_0)$ upon varying k_4, k_6, k_7 and k_9. As expected, changing the catalytic rate k_9 has the largest effect on the response curve.

The parameters k_{10}, k_{12}, k_{13}, and k_{15} are rate constants associated with reactions of CheZ that is bound to the cluster; these rate constants correspond to, respectively, k_4, k_6, k_7 and k_9 of reactions of CheZ in the cytoplasm. As such, the effect of varying the parameters k_{10}, k_{12}, k_{13} and k_{15} on the response curve can be deduced from the effect of changing the parameters k_4, k_6, k_7 and k_9, discussed above. However, since CheZ bound to the

cluster is present in low concentrations, and has a much higher affinity for $CheY_p$ and a higher catalytic activity, the magnitude of the effect is markedly different. In particular, changing k_{10}, k_{12} and k_{13} hardly has any effect. This is because CheZ at the cluster is strongly driven to the $(CheY_p)_2CheZ$ state. For precisely the same reason, the largest effect is observed for changes in the catalytic rate k_{15}.

The last graph in Fig. 4 shows the effect of varying the diffusion coefficient D. The diffusion coefficient is assumed to be equal for all diffusive components. A decrease in D has the effect that larger gradients of $CheY_p$ arise. As a consequence, the concentration of $CheY_p$ integrated over the whole cell decreases. Since also larger gradients of Y_pZ and $(Y_p)_2Z$ occur, the total concentrations of Y_pZ and $(Y_p)_2Z$ decrease as well for lower values of the diffusion constant; this explains the decrease in FRET signal with decreasing diffusion constant.

[1] Blat Y, Eisenbach M (1996) Oligomerization of the phosphatase CheZ upon interaction with the phosphorylated form of CheY. J Biol Chem 271:1226–1231.

[2] Blat Y, Gillespie B, Bren A, Dahlquist FW, Eisenbach M (1998) Regulation of phosphatase activity in bacterial chemotaxis. J Mol Biol 284:1191–1199.

[3] Silversmith RE, Smith JG, Guanga GP, Les JT, Bourret RB (2001) Alteration of a nonconserved active site residue in the chemotaxis response regulator CheY affects phosphorylation and interaction with CheZ. J Biol Chem 276:18478–18484.

[4] Silversmith RE, Levin MD, Schilling E, Bourret RB (2008) Kinetic Characterization of Catalysis by the Chemotaxis Phosphatase CheZ. J Biol Chem 283:756–765.

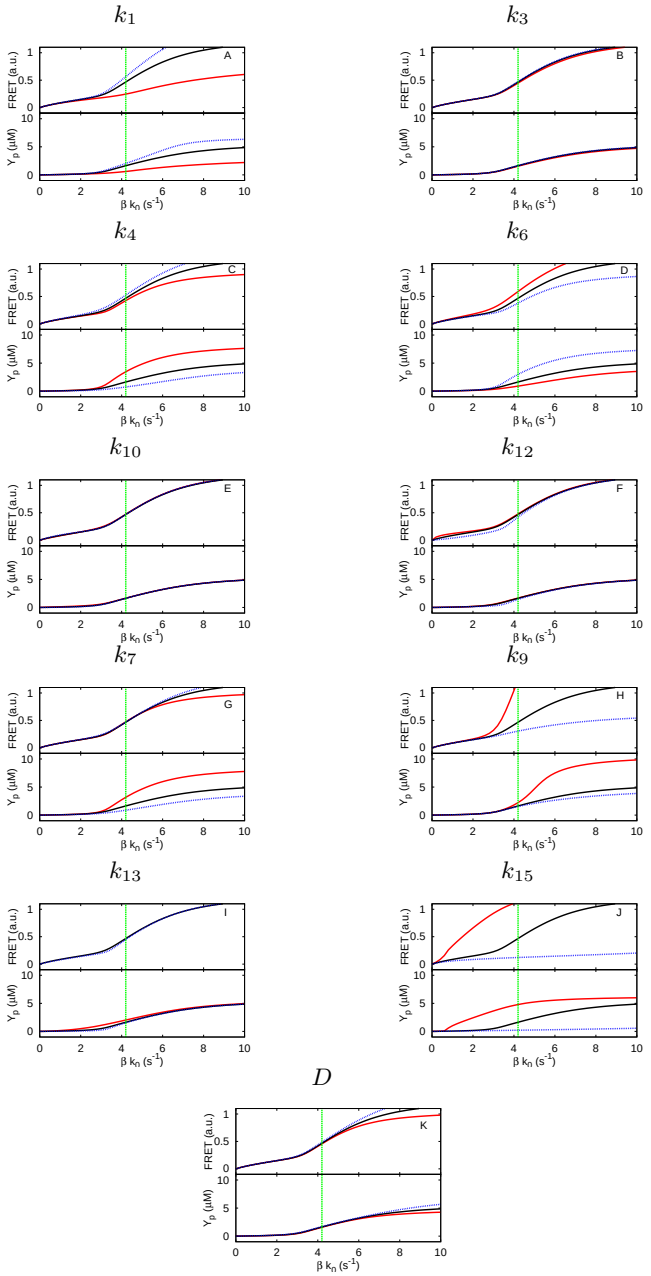

FIG. 4: The effect of varying the different parameters of the full model of the intracellular chemotaxis network (Equations 8–13) on the response curves $[\mathrm{Y_p}](\beta k_0)$ and $\mathrm{FRET}(\beta \mathrm{k_0})$; here $\mathrm{FRET} \propto [\mathrm{Y_pZ}] + 2[(\mathrm{Y_p})_2\mathrm{Z}] + [\mathrm{Y_pZ_b}] + 2[(\mathrm{Y_p})_2\mathrm{Z_b}]$. The baseline parameters are $k_1 = 3\ 10^6\ \mathrm{M^{-1}s^{-1}}$, $k_3 = 750\ \mathrm{s^{-1}}$, $k_4 = 3.6\ 10^5\ \mathrm{M^{-1}s^{-1}}$, $k_6 = 7.5\ \mathrm{s^{-1}}$, $k_{10} = 6\ 10^8\ \mathrm{M^{-1}s^{-1}}$, $k_{12} = 40\ \mathrm{s^{-1}}$, $k_7 = 3\ 10^7\ \mathrm{M^{-1}s^{-1}}$, $k_9 = 30\ \mathrm{s^{-1}}$, $k_{13} = 9\ 10^8\ \mathrm{M^{-1}s^{-1}}$, $k_{15} = 160\ \mathrm{s^{-1}}$, $D = 5\ \mu\mathrm{m^2s^{-1}}$, $[\mathrm{Y}]_\mathrm{T} = 17.9\ \mu\mathrm{M}$, $[\mathrm{Z}]_\mathrm{T} = 1\ \mu\mathrm{M}$, $[\mathrm{Z_b}]_\mathrm{T} = 0.1\ \mu\mathrm{M}$ and $[\mathrm{A}]_\mathrm{T} = 5\ \mu\mathrm{M}$. The parameter values are 0.2 (red), 1 (black) and 5 (blue) times the baseline parameters. Exceptions are $k_{13} : k_{13} = 1.8\ 10^8,\ 6\ 10^9$ and $3\ 10^{10}\ \mathrm{M^{-1}s^{-1}}$ and the diffusion coefficient: $D = 3$ (red), 5 (black) and 10 $\mu\mathrm{m^2s^{-1}}$ (blue). The vertical green lines indicate the non-stimulated state for the baseline parameter set.